Defects in Bent-core Liquid Crystals

Antal Jákli[1,*], Yuriy Nastishin[2] and Oleg D. Lavrentovich[1]

[1]*Department of Physics, Materials Sciences Graduate Program, Advanced Materials, and Liquid Crystal Institute, Kent State University, Kent, OH, 44242, USA*

[2]*Hetman Petro Sahaidachnyi National Army Academy, Heroes of Maidan St. 32, Lviv 79012, Ukraine*

ABSTRACT:

Topological defects and defect phases of rigid and flexibly bent-shaped liquid crystals are reviewed with emphasis on how they are affected by the departure of molecular shapes from a simple rod. The review discusses defects in bent-core uniaxial and hypothetical biaxial nematics, twist-bend nematic, and various frustrated layered bent-core liquid crystals, such as twist-grain boundary phase, nanoscale helical nanofilament phase, and the so-called B_7 textures with helical ribbons.

1. INTRODUCTION

The spatial organization of liquid crystals (LCs) is governed by molecular shapes and interactions and reveals itself at the macroscopic scale by anisotropic properties and various textures with an abundance of topological defects. LC defects, representing singular and non-singular distortions of the orientational order, carry signatures of the undistorted ground LC state and bear specific information that helps to identify phases in newly synthesized materials. It was the line defect-disclinations that prompted G. Friedel to assign the name "nematic" to the simplest LC, the uniaxial nematic (N_U), and it was the focal conic domains (FCDs) that revealed to him the layered molecular-scale organization of smectics [1]. Small variations of molecular shapes produce remarkable changes in the self-assembly of liquid crystalline phases, as demonstrated by the discovery of the twist-bend nematic formed by flexible dimers, which represent two rod-like molecules connected by a flexible aliphatic bridge of a bent conformation; if the bridge is straight or absent, the molecules form a conventional N_U. Uncovering properties of LCs and defects in them is not a simple task, as it involves, citing P.G. de Gennes, "a certain sense of vision in three-

dimensional space in order to visualize complex molecular arrangements."[2] Maurice Kleman was one of the pioneers in the field, whose vision laid a foundation for the modern knowledge of defects in LCs and other ordered media, summarized in his monograph [3,4] and reviews [5–11].

"So full of shapes is fancy,
That it alone is high fantastical."

These lines by William Shakespeare from Twelfth Night [I, 1, lines 14-15], were selected by Maurice Kleman as an epigraph to the paper [12] , to express the richness of geometrical forms associated with defects in LCs formed by bent-core molecules. The choice reflects his life-long fascination with defects in condensed matter, which resulted in remarkable achievements, including elucidation of the fine structure and properties of line defects in cholesterics [5,13,14], uniaxial [15], twist-bend [16], and biaxial nematics [17], thermotropic [18–25] and lyotropic smectics [26–28], columnar [29,30] and twist-grain-boundary [31,32] phases, predictive descriptions of FCDs in smectics [26,33,42,34–41], and developable domains [43,44] in hexagonal columnar liquid crystals, general classification of defects in ordered media by the homotopy group theory [45–47].

This review explores how the topological signatures of defects in LCs are affected by the departure of molecular shapes from a simple rod. The focus is on the bent shape, which resembles a boomerang or a banana. Flexible dimers are the most recent addition to this family, although they are "bent-bridge" rather than bent-core mesogens. In Chapter 2 we discuss defects in bent-core uniaxial and hypothetical biaxial nematics, Chapter 3 is devoted to the description of defects in the twist-bend nematic, and Chapter 4 summarizes the studies of defects in various frustrated bent-core LCs, such as twist-grain boundary phase, nanoscale helical nanofilament phase (HNF), and the so-called B_7 textures with helical ribbons. Chapter 5 provides an outlook.

2. UNIAXIAL AND BIAXIAL NEMATIC PHASES

Focused studies of the defects in the uniaxial nematic (N_U) phase of bent-core molecules are scarce. A notable exception is the exploration of twist disclination loops by Krishnamurthy, Tadapatri, and Weissflog. [48] These loops, first introduced in the theoretical paper by Friedel and de Gennes [49], are topologically trivial in the sense that they could shrink into a uniform state. They separate a twisted state from the planar state. Depending on whether the twisted state is in the interior or exterior, one distinguishes L(T) and L(P) loops, respectively, Figure 1(a).

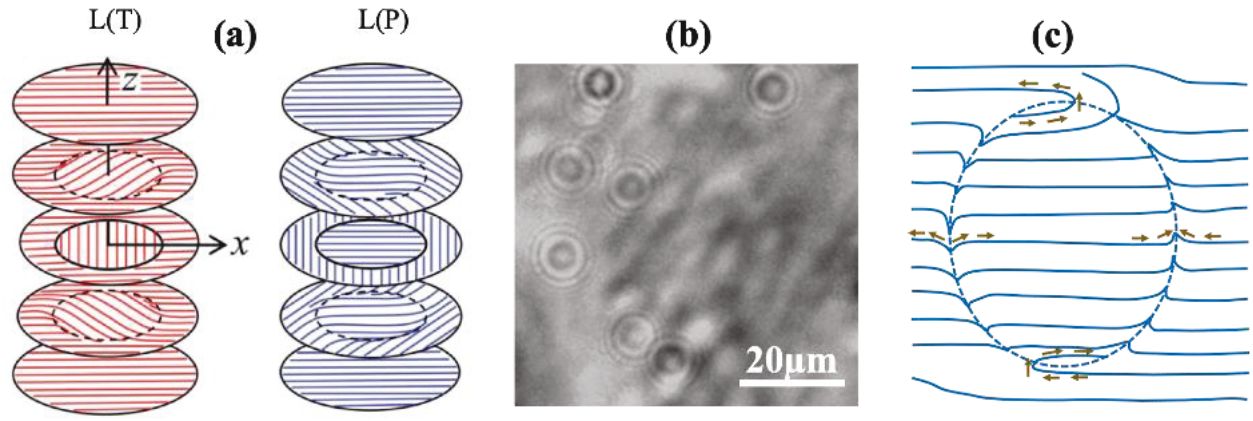

Figure 1:(a) Twist disclination loops in a planar nematic cell. The L(T) disclination encloses the twisted state, and L(T) loop encloses the planar state. (b)Disclination loops observed in the N_U phase of BCN films while cooling in the presence of uniform external field. (c) Schematic director structure around the loop.

Both types could be created by abruptly applying an electric field to an initially planar cell along the direction perpendicular to the plates coated with transparent electrodes and then switching the field off. Relaxation of the director field produces L(T) or L(P) loops; the latter are formed when the electric voltage exceeds significantly the Frederiks threshold. L(T) loops inevitably shrink to leave a uniform planar state since their energy decreases monotonically in the process. In contrast, L(P) loops behave similarly to the nuclei in the first-order phase transition. They expand or shrink, depending on whether their initial radius R is larger or smaller than some critical value. This behavior is rooted in the elastic energy $F \propto K[Rln(R/r_c) - \pi R^2/d]$ of an L(P) loop, where K is a representative Frank elastic constant, r_c is the core radius of the disclination, d is the cell thickness. The term approximately linear in R represents the line tension of the disclination, while the R^2 term is the gain in the elastic energy when the twisted state is replaced by a uniform planar one. The energy balance is similar to the balance of surface tension $\propto R^2$ and internal energy $\propto R^3$ in the nucleation problem. As stressed by the authors of Ref. [48] , the behavior is not exclusive to the bent-core N_U, as similar features are observed in rod-like N_U, with an understandable difference in materials parameters such as elastic constants and viscosity coefficients.

Different splay-bend defect loops were observed in the N_U phase of thick bent-core nematic (BCN) samples while cooling from the isotropic phase in the presence of a uniform magnetic field **H**. [50] Figure 1b reveals multiple micron-scale defect loops. Inside and outside every loop, $\hat{\mathbf{n}}$ is parallel

to **H**, but it is distorted across the boundary, Figure 1c. These features are characteristic of *inversion wall loops* [51]. The inversion walls form in the presence of an external field or surface anchoring that forces the director to align along a single direction in space [4], e.g., $\pm\hat{\mathbf{n}}||\mathbf{H}$ in the experiment [50]. Under this constrain, the inversion walls are topologically equivalent to Néel and Bloch walls in ferromagnets, in which the two opposite directions of magnetization are set by crystal anisotropy [52]. The inversion wall separates two domains with antiparallel orientations $\hat{\mathbf{n}}$ and $-\hat{\mathbf{n}}$; across the wall,the director realigns by π In the Néel type, $\hat{\mathbf{n}}$ rotates around an axis perpendicular to both the wall and the director, forming splay or bend distortions, both of which generate a flexoelectric polarization [53], rendering the local wall structure non-centrosymmetric, despite the centrosymmetric nature of an undistorted N_U.

A strong effect of elastic constants on the structure of defects is observed in N_U formed by acute-angle bent-core molecules of a shape resembling a letter λ, Figure 2a [54]. The measured splay elastic constant is anomalously weak, $K_{11} = 2$ pN, significantly smaller than the bend constant $K_{33} = 15$ pN and even the twist constant $K_{22} = 5$ pN. The smallness of K_{11} leads to a pronounced bias of defects towards configurations with splay, in the nuclei emerging from the isotropic phase, Figure 2b, and in Schlieren textures, Figure 2c [54].

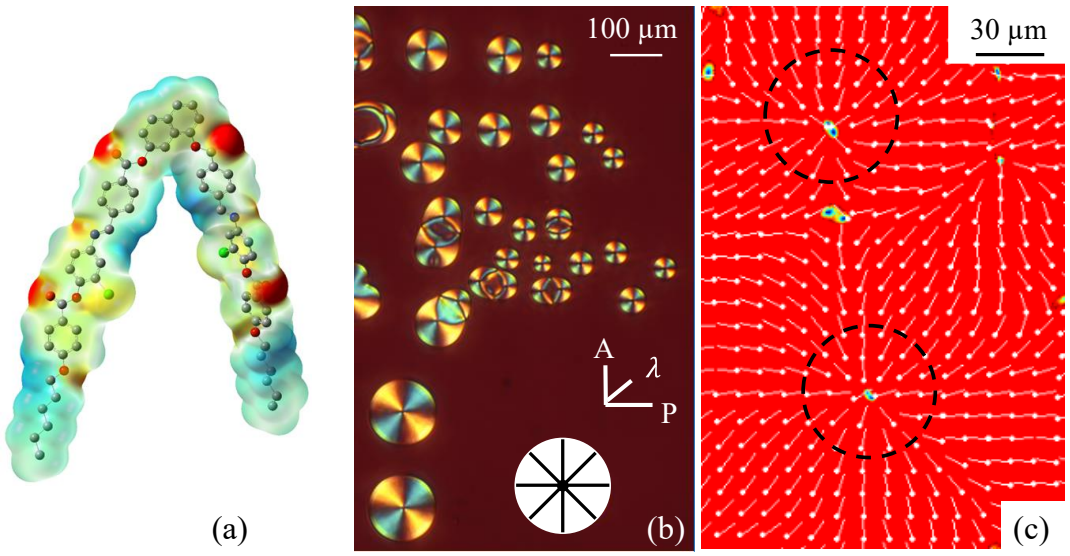

Figure 2: (a) Acute-angle bent-core molecule 1,7-naphthylene bis(4-(3-chloro-4-(4-(hexyloxy)benzoyloxy)phenyliminomethyl) benzoate) forms N_U with a small splay elastic modulus, which results in prevalence of splay deformations in (b) N_U nuclei forming on cooling from the isotropic phase and (c) Schlieren textures; +1 defects surrounded by dashed circles are of radial type.

Although the bent-core LCs have been known for about a century, see Ref. [55] for a brief review, the explosion of interest to them happened only after the rod-like N_U counterparts have already demonstrated spectacular performance in LC displays. The idea was to find a biaxial nematic N_B, which could be switched faster and by a lower electric field than N_U. Bent-core molecules seemed to be natural candidates, as the secondary director could be associated with the "cusp" of the shape. The N_B phase was theoretically described by Freiser [56] as being of orthorhombic symmetry with physical properties different along three mutually perpendicular directors $\hat{\mathbf{n}} \equiv -\hat{\mathbf{n}}$, $\hat{\mathbf{m}} \equiv -\hat{\mathbf{m}}$, and $\hat{\mathbf{l}} \equiv -\hat{\mathbf{l}}$.

To this day, however, the existence of N_B in thermotropic systems remains elusive, despite the intense search. First, Li et al.[57] demonstrated the N_B phase in a material formed by cyclic (ring-like) molecules. The search expanded to bent-core molecules after Niori et al. [58] showed that they could form a biaxial smectic. The difficulty in identifying N_B is that most of the experimental techniques test the properties of the material averaged over the sample bulk [55]. As a result, the presence of inhomogeneities, such as deformations of the uniaxial director $\hat{\mathbf{n}}$, caused by anchoring transitions [59–61], or by flows triggered by thermal expansion [62,63], could be erroneously interpreted as an apparent biaxiality. In some cases, the remedy is simple. For example, one could apply an electric field to align $\hat{\mathbf{n}}$, and then explore whether the material is birefringent in the orthogonal plane [59,60]. However, when the material of a negative dielectric anisotropy (measured with respect to $\hat{\mathbf{n}}$), this approach would not discern between N_U and N_B.

A robust approach to test the long-range biaxial order, alternative to the volume-averaging techniques such as optical conoscopy, X-ray, or NMR, is through topological defects, especially those that correspond to the equilibrium ground state of the mesophase in confined geometries. Line defects (disclinations) and point defects (hedgehogs and boojums) in N_U and N_B show dramatic differences as discussed below.

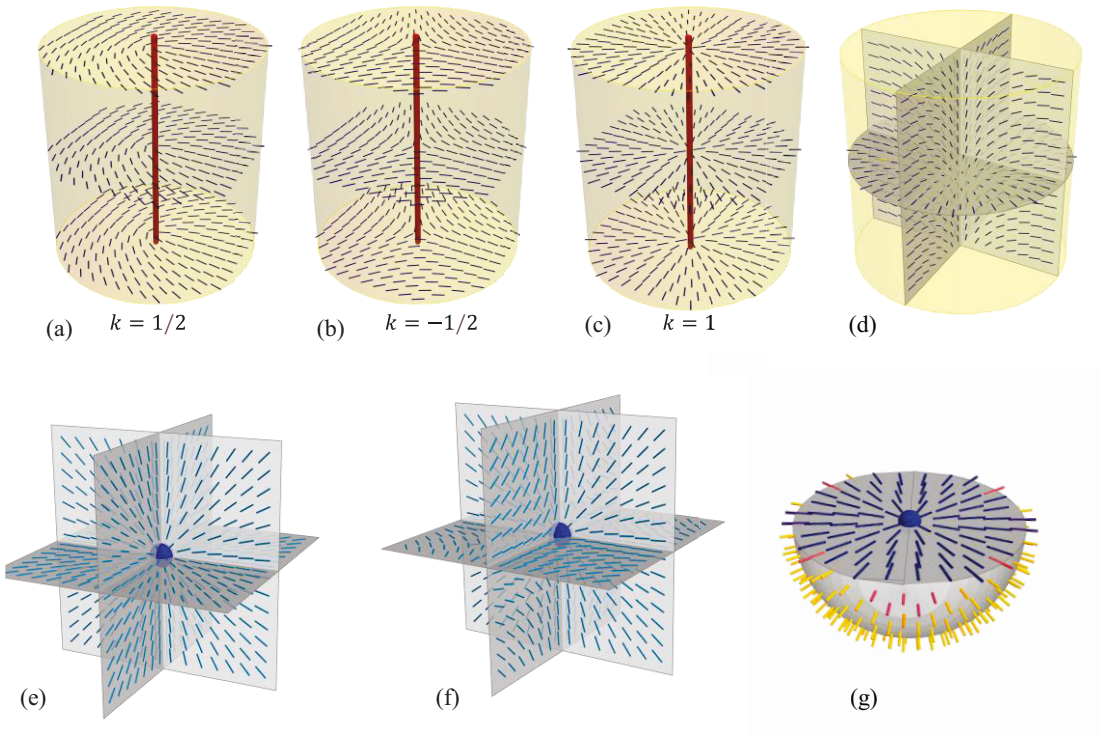

Figure 3: Topological defects in N_U. Stable disclinations of strength (a) $k = 1/2$ and (b) $k = -1/2$ with singular cores; (c) topologically unstable disclination $k = 1$, which are continuously transformable into (d) a non-singular "escaped" configuration with the director along the initial core. (e) Radial and (f) hyperbolic point defects-hedgehogs in the bulk; (g) radial boojum at the surface of N_U.

In the N_U bulk, the topologically stable defects are disclination lines of strength $|k| = \frac{1}{2}$, where k is defined as a number of director turns by 2π when one circumnavigates the defect core once, Figure 3a,b. Disclinations of strength $|k| = 1$ are not topologically stable; a realization that first came on the ground of elastic energy minimization by Cladis and Kleman [15] and independently by Meyer[64] and later through the homotopy groups concept [33,47,65]. As an example, Figure 3c,d shows that the singular core of a $k = 1$ disclination could be removed by simply realigning the director along the disclination's axis. In the process of realignment, the elastic energy of the disclination decreases monotonously [15,65]. The effect was called "the escape into the third dimension" by R.B. Meyer [64]. N_U also exhibits two different types of point defects [66], (i) hedgehogs that can exist in the N_U bulk, Figure 3e,f, or at its surfaces and (ii) boojums that exist only at the surface of N_U, Figure 3g [66]. A detailed overview of defects in N_U is presented in this special issue by Harkai et al. [67]

In N_B, the line disclinations with a singular core are stable whether $|k| = \frac{1}{2}$ or 1. The reason why a disclination of strength $|k| = 1$ could not be removed by the "escape into the third dimension" is that the reorientation of one director ($\hat{\mathbf{n}}$ in Figure 4a) along the disclination's axis brings two other directors (for example, $\hat{\mathbf{m}}$ in Figure 4a) into a singular geometry [68]. One of the fascinating features of defects in N_B, predicted by Toulouse [68] , is that crossing of two disclinations of strength $|k| = \frac{1}{2}$ can result in the appearance of a $|k| = 1$ disclination that connects these two, Figure 4b. Since the elastic energy of disclinations is proportional to their length, the interaction potential of two $k = \frac{1}{2}$ disclinations connected by a line $k = 1$ of a length L is $U \propto KL$, similar to the interaction of quarks. In N_U, disclinations cross each other freely [45] Observation of the nontrivial crossing would be an ultimate test of the N_B existence, but the crossing of disclinations has been so far studied only in N_U [69] .

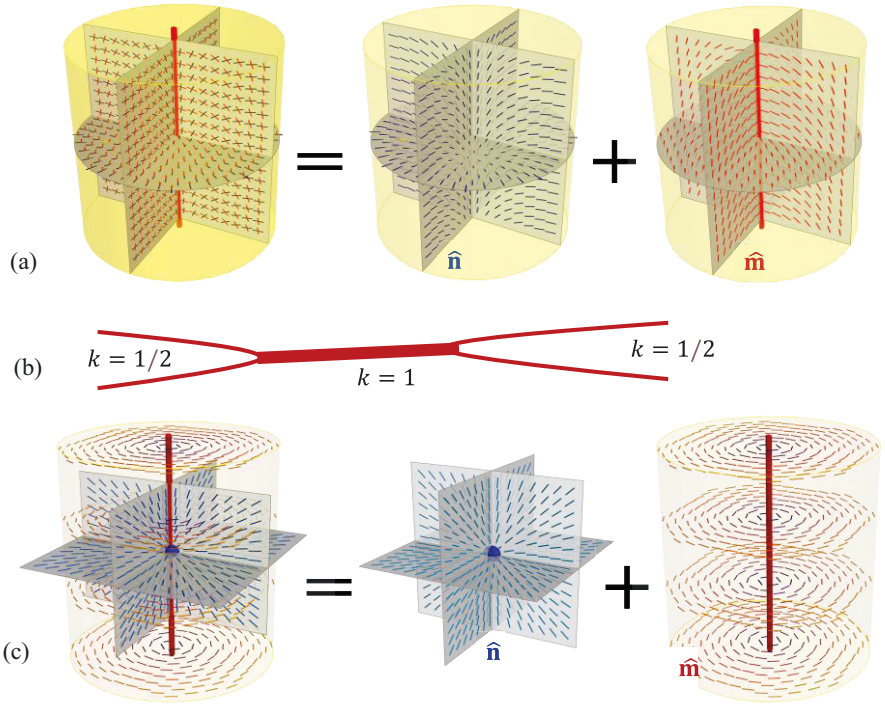

Figure 4: Topological defects in N_B. (a) Removal of a singular core through the escape of the director $\hat{\mathbf{n}}$ into the third dimension of a $k = 1$ disclination is impossible since the realignment of $\hat{n}$ brings another director, $\hat{\mathbf{m}}$, into a singular core. (b) Two $k = 1/2$ disclinations of connected by a singular $k = 1$ line interact similarly to quarks. (c) Isolated point defects-hedgehogs could not exist in N_B since they should be attached to disclinations.

Point defects provide another opportunity for an experimental test of bulk biaxial order. Isolated point defects cannot exist in N_B, Figure 4c. For example, a radial configuration of one director implies that the two other directors are defined at a spherical surface and thus should form additional singularities emanating from the center of the defect, similarly to the famous "Dirac monopole" with a radial point defect-hedgehog in the magnetic field and an attached string in the vector-potential that is perpendicular to the field [70]. Surface point defect-boojums of strength $|k_b| = 1$ also cannot exist, as they must be connected to a singular bulk disclination of the same strength $|k| = 1$ [68], and thus represent the ends of these disclinations rather than isolated points. References [55,71] present detailed illustrations and suggest experiments that might reveal the existence of N_B through the analysis of topological defects in crossings and in confined geometries, such as cylindrical capillaries, freely suspended droplets, and LC slabs containing colloidal particles.

Some of the topology-based tests of the potential biaxiality of bent-core nematics have been already performed and resulted in a conclusion that the studied materials are of the N_U rather than the N_B type. In particular, cylindrical capillaries with perpendicular director anchoring at the walls, filled with the bent-core mesogens, such as A131[60] C7 and C12[72] show that the director $\hat{\mathbf{n}}$ realigns smoothly along the capillary axis, Figure 3d and does not produce a singular core expected for the N_B phase, Figure 4a.

3. DEFECTS IN TWIST-BEND NEMATIC (N_{TB}) PHASE

While the bent-core mesogens did not provide clear evidence of the existence of N_B, flexible dimers revealed a no less interesting new phase, the twist-bend nematic (N_{TB}) [73–75] , predicted by R.B. Meyer [76], I. Dozov [77], and R. Memmer [78]. Flexible dimers with a bridge comprised of an odd number of methylene groups tend to adopt bent conformation. If these molecules fill a 3D space, this bend could be preserved unchanged throughout only if accompanied by splay or twist deformations. The latter case produces the N_{TB} phase, Figure 5. The local director $\hat{\mathbf{n}}$ is tiled with respect to the heliconical axis $\hat{\boldsymbol{\chi}}$; its projection onto the plane orthogonal $\hat{\boldsymbol{\chi}}$ to is $\hat{\boldsymbol{\lambda}}$; one also defines the orthogonal vector $\hat{\boldsymbol{\tau}}$, so that $\hat{\boldsymbol{\lambda}} = \hat{\boldsymbol{\chi}} \times \hat{\boldsymbol{\tau}}$. The planes of the constant phase of the tilt should be equidistant, otherwise the bend and twist deformations should deviate from the equilibrium values, which would cost some elastic energy, associated with a non-vanishing Young's modulus. This equidistance of pseudo-layers is not associated with any density

modulation. The N_{TB} structure is therefore similar to the density-modulated smectic C* (SmC*), and pseudo-layered cholesteric (Ch) and especially the oblique helicoidal state of the cholesteric (Ch_{OH}), which forms in chiral flexible dimer Ch under the action of an external electric or magnetic field [79–82]. The pitch of Ch_{OH}, defined by the chirality of constituent molecules, is usually in the submicron and micron range, i.e., much larger than the pitch p of N_{TB}, which is only about 10 nm, as determined by the freeze-fracture TEM studies [74,75].

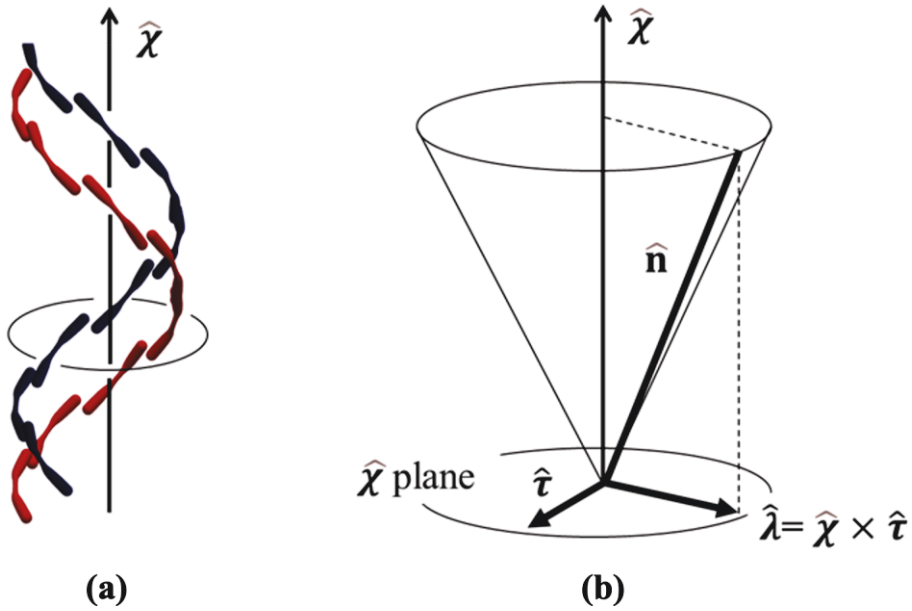

Figure 5:Schematic structure of the N_{TB} phase: (a) Molecular arrangements; (b) Definition of the trihedron: $\hat{\boldsymbol{\chi}}$ is the heliconical axis, $\hat{\boldsymbol{\lambda}}$ is the projection of the local director onto the plane orthogonal to $\hat{\boldsymbol{\chi}}$; $\hat{\boldsymbol{\tau}}$ is normal to both $\hat{\boldsymbol{\lambda}}$ and $\hat{\boldsymbol{\chi}}$.

Kleman and Krishnamurthy[16] classified linear defects in N_{TB} by exploring its elements of symmetry. These are (i) quantized, or perfect, dislocations of the Burgers vector np, (ii) quantized disclinations of the Frank vector $(\pi + 2m\pi)\hat{\boldsymbol{\tau}}$; here n and m are integers; (iii) continuous dislocations with infinitesimal Burgers vectors in the planes orthogonal to $\hat{\boldsymbol{\chi}}$; (iv) continuous dispirations, i.e., combinations of disclinations of infinitesimal Frank vector and infinitesimal Burgers vector. The classification is the same as for Ch, except that in Ch, there are also quantized disclinations with the Frank vector parallel to the local director $\hat{\mathbf{n}}$, which is in the planes orthogonal to $\hat{\boldsymbol{\chi}}$ [16]. Pieranski [83] and Wu and Smalyukh [84] provide extensive reviews of defects in Ch.

Alongside linear defects, which are typically hard to observe directly because of the small pitch, which usually defines the size of the "core" of linear defects, the pseudo-layered structure of N_{TB} leads to macroscopic-scale textures and defects similar to those in other layered systems, such as stripes and FCDs, both of extension orders of magnitude larger than the pitch p ~10 nm. These are discussed below.

3.1. Textures as evidence of the pseudo-layered structure of N_{TB}.

The first clear hint that nematic materials could form a new phase, identified later as N_{TB} [73–75], came from the observation of stripe textures by Panov et al.[85], later confirmed by others [73,86–92]. Figure 6a,b show these stripes along the rubbing direction in the planar cell filled with a mixture CB9CB+5CB (60:40 wt%). Panov et al. [85] noted that the stripes occur in relatively thin cells (10 μm or less), and their period is about twice the cell thickness. In thicker samples, one often observes FCDs, elongated along the rubbing direction, Figure 6e. The stripes are characteristic of practically all N_{TB} samples, including droplets[92]; they are not topologically stable in the sense that a strong field could eliminate them, Figure 6c,d [88].

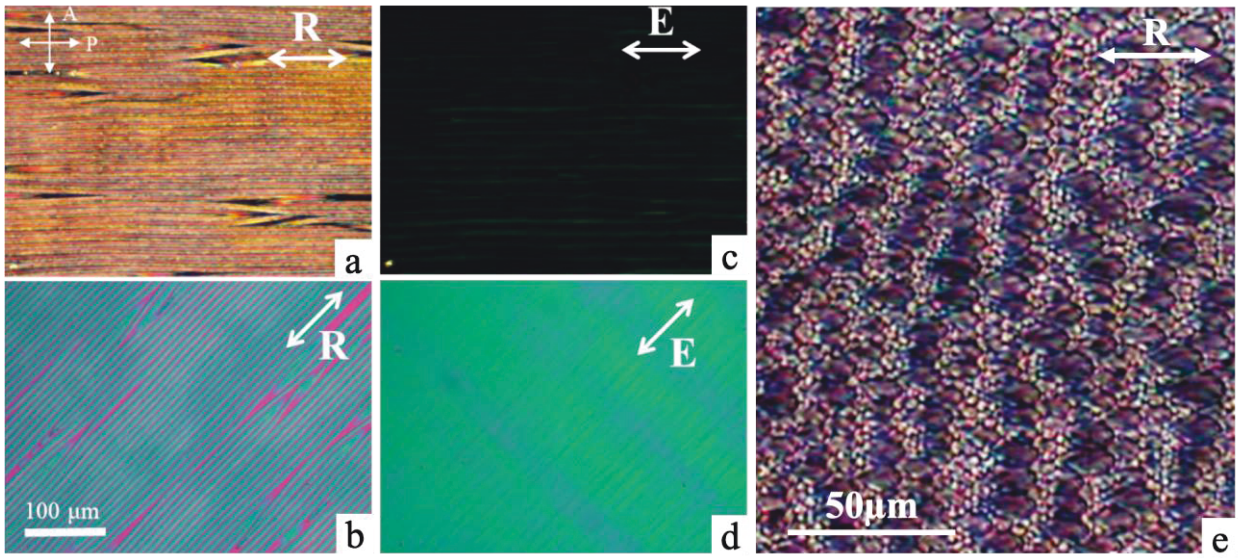

Figure 6: Typical polarizing optical microscopy textures of N_{TB} phase in planar samples: (a,b) stripe pattern parallel to the rubbing direction R, cell thickness 7 μm; (c,d) in-plane AV electric field eliminates the stripes; (e) focal conic domains, cell thickness 20 μm. Material: Mixture of CB9CB+5CB, 60:40 wt%. The material was provided by Vitaly Panov and Georg Mehl. Experimental data by Young-Ki Kim (unpublished).

The textures of stripes are ubiquitous in systems with one-dimensional stacking of flexible equidistant layers. They indicate the tendency of layers to tilt in response to mechanical stress,

such as temperature-induced variation of the period or an external field [4]. The underlying physics is captured by the so-called Helfrich-Hurault (HH) buckling instability [2], usually invoked when the layers are parallel to the bounding plates of the cell. However, the general mechanism of the HH buckling remains valid even when the layers are perpendicular to the bounding plates. In such "bookshelf" geometry, the tilt of smectic layers typically occurs across the cell ("vertical chevron") [93], but it is also observed in the plane of the cell [93,94]. The latter "horizontal chevron" texture is similar to the N_{TB} stripes. This similarity and disappearance of the stripes at a high magnetic field allowed Challa et al. [88] to explain the stripe formation by the HH mechanism, i.e., as a result of the temperature-dependent N_{TB} pitch. Polarizing microscopy and fluorescence confocal polarizing microscopy (FCPM) study by You et al. [89] suggests that the heliconical axis in stripes experiences predominantly splay, tilting left and right from the direction set by rubbing. Similar splayed configurations are observed by Panov et al. [90] in scanning electron microscopy of polymer-stabilized N_{TB} [90] . The prevalence of splay is expected, as the N_{TB} structure that keeps the equidistance of pseudo-layers allows splay of the normal $\hat{\boldsymbol{\chi}}$ to the layers but hinders bend and twist (which are present at the molecular scale of the local director, hence the name).

FCD textures are a hallmark of layered LCs. These domains, often appearing as pairings of ellipses and hyperbolae, were the first textures of LCs Kleman viewed in the late 1960-ies under a polarizing microscope. [95] Since early studies of smectics, thanks to the insights of G. Friedel and F. Grandjean in 1910 [96], the appearance of the FCDs was attributed to one-dimensionally periodic stackings of flexible layers; the conclusion formed a cornerstone of George Friedel's classification of LC phases [1]. The conclusion was made well before X-ray studies by Edmond Friedel, son of George Friedel, could confirm the one-dimensional density variation of smectics with a layer's thickness being only a few nanometers. A son of Edmond, Jacques Friedel, became a prominent condensed matter scientist known most for the studies of dislocations in solids [97]. He was also an adviser of Kleman's thesis and a long-time collaborator [3,5]. For the history of science of defects in condensed matter see the paper by T. Sluckin in this special issue [84]. Kleman expanded G. Friedel's geometrical constructions of FCDs by developing an analytical description of FCDs and their associations [3,33]. The theory yields the general expression for the energy of the domains and demonstrates the relation of FCDs to grain boundaries and dislocations [3,33,40,41]. FCDs in N_{TB} are more complex than the well-studied FCDs in smectic A. These complexities were analyzed by Kleman in his last papers, written in collaboration with

Krishnamurthy and other colleagues [16,98,99]. Below we review the general properties of FCDs and then discuss the peculiarities of FCDs in N_{TB}.

3.2. General properties of FCDs.

FCDs relieve curvature energy of layers subject to boundary conditions or external fields. Curved layers tend to preserve perfect parallelism in order to avoid large compression/dilation energy associated with the change of their thickness. Curved parallel layers cannot fill space continuously, as the radii of curvature tend to zero at some locations, which for 3D space are 2D surfaces, called focal surfaces. These surfaces represent the loci of the centers of curvature. At the focal surfaces, the normal to layers experiences singularity; in the physical context of ordered media, focal surfaces carry significant elastic energy proportional to their area. The simplest solution is to reduce the dimensionality to focal lines. Families of curved parallel layers with focal lines are known in mathematics as Dupin cyclides; in LCs, the cyclides represent the curved equidistant layers. In 1868 Maxwell found solutions in the form of Dupin cyclides while solving a problem (similar in many respects to that of FCDs) of wave surfaces propagating along rectilinear rays in an isotropic medium [99].

By geometrical construction, the focal lines must be pairs of conjugated conics. The most common example is a pair of an ellipse and a branch of a hyperbola located in mutually orthogonal planes, such that the apices of one are the foci of the other. These form FCDs of the so-called first, Figure 7, second, and third species, classified on the basis of whether the curved layers are of a negative Gaussian curvature (FCD-I), positive Gaussian curvature (FCD-II), or both negative and positive Gaussian curvatures (FCD-III), respectively [4]. Figure 7 illustrates that the layers' curvatures diverge at the ellipse and hyperbola so that these conics represent singularities in the field of normals to the cyclides. Layers could also wrap around conics without singularities, as the middle cyclide does in Figure 7a. Any line connecting the hyperbola to the ellipse is normal to the layers; in the case of smectics, this line coincides with the director $\widehat{\mathbf{n}}$; in the case of N_{TB}, it is the axis $\widehat{\boldsymbol{\chi}}$ of heliconical twist. Dupin cyclides corresponding to the ellipse-hyperbola frame are parametrized in Cartesian coordinates as [40]

$$x = \frac{r(c - a\cos u\cos v) + b^2\cos u}{a - c\cos u\cos v}; y = \frac{b\sin u(a - r\cos v)}{a - c\cos u\cos v};\ z = \frac{b\sin v(c\cos u - r)}{a - c\cos u\cos v};$$

where a and b are the major and minor semi-axes of the ellipse, respectively, $c^2 = a^2 - b^2$, u and v are the two orthogonal angular coordinates specified at the cyclides, and r is the third coordinate along the normal to the cyclides. The range of values (r, u, v) determines whether the resulting cyclides would be of a positive or negative Gaussian curvature and whether they will be complete or not.

All the cyclides in FCD-Is, Figure 7, have negative Gaussian curvature, which is preferable by elasticity: the opposite signs of the principal curvatures imply a smaller splay energy, which is determined by the square of the mean curvature. The mean curvature is the algebraic sum of the principal curvatures. A rare example of an FCD-II has been observed in lyotropic lamellar phases [36,37].

The FCD-Is limited by conical shapes with an elliptic base are often met in polygonal textures in which surface anchoring aligns the director tangentially to the substrates, as first demonstrated by Bragg [100]. This anchoring effect is illustrated in Figure 7b: the normal to the layers within an ellipse is everywhere in the plane of the ellipse. The polygonal textures of FCD-Is form a hierarchy, with ellipses of smaller domains placed between the larger domains; the packing of ellipses shows fractal dimension [101]. Gaps between the cones are filled with a layer of a spherical shape and thus positive Gaussian curvature [35,102]. The largest domains in the fractal structure are of the size dictated by the cell thickness, while the smallest are defined by the balance of the elastic and surface anchoring energy [102].

FCD-Is sometimes reduce to a toroidal FCD (TFCD), in which the ellipse becomes a circle, $a = b, c = 0$, and the hyperbola is a straight line passing through the center of the circle, Figure 7c. The TFCD could be smoothly extended by a system of flat layers parallel to the circular base. Within a TFCD, the principal radii, shown by red vectors in Figure 7c, are of the opposite signs, as in any FCD-Is of negative Gaussian curvature. TFCDs could occur not only because of the surface anchoring, but also because of the external field that aligns the director perpendicular to itself. [38,103]

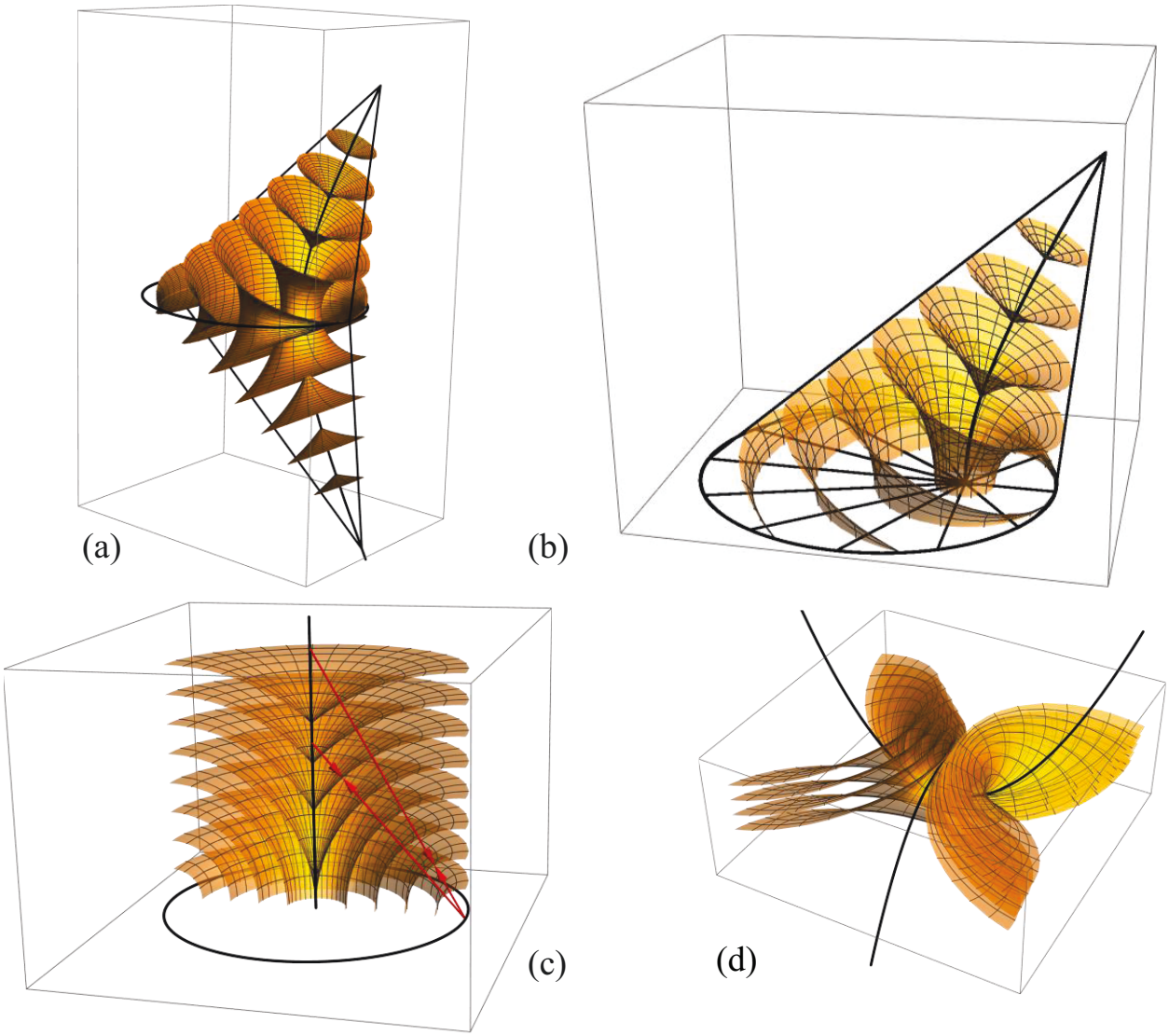

Figure 7: Focal conic domains (FCDs) of first species: (a) FCD-I with negative Gaussian curvature of the Dupin cyclides (layers) limited by conical surfaces and an elliptical base; (b) FCD-I with the elliptic base at a substrate that prefers a tangential alignment of the normal to the layers; these shapes form the so-called polygonal textures in many layered liquid crystals; (c) TFCD with the ellipse degenerate into a circle and the hyperbola straightened up into a line passing through the center of the circle; the arrows show the principal radii at two points; the Gaussian curvature is negative since the radii are antiparallel; (d) parabolic focal conic domain.

Finally, a distinct class of FCDs are parabolic FCDs (PFCDs), in which the conics represent two confocal parabolas [104], Figure 7d. PFCDs usually occur under dilative mechanical stresses [104], or when the layer thickness decreases as a result of temperature change or *cis-trans* isomerization [105]. The reason is that the same layer crosses the normal to the cell substrates three times close to the PFCD's axis, thus filling the space created by dilations.

TFCDs and PFCDs occur in bent-core layered mesophases alongside FCD-Is. The prevalence of one type over the other is controlled by elastic and surface anchoring properties. TFCDs are observed in a biaxial SmA, formed by a mixture of rod-like and bent-core molecules [106]. TFCDs also emerge as an intrinsic element of the dark conglomerate (DC) phase, which is a chiral isotropic liquid [107]; they appear in the bulk [107] and at the free surfaces of the DC samples [108,109]. PFCDs are observed in the B_4 phase, in which bent-core molecules build up helical nanofilaments driven by a negative Gaussian curvature. They appear either near glass substrates [110] or at the free surface [109].

3.3. FCDs in N_{TB}.

Figure 8 illustrates a light-induced reversible transformation between N_{TB} and N_U heralded by recurrent disappearance and reappearance of FCD-Is [111]. The N_{TB} transformation into N_U is triggered by UV irradiation in a material formed by flexible dimers that contain azobenzene groups. UV creates an excess of *cis*-isomers of a zig-zag shape that are not compatible with the prevalent bend of the *trans*-isomers. Once the UV irradiation is stopped, the molecules relax to properly bend *trans*-forms, restoring N_{TB}, as manifested by the resurrection of FCD-Is [111,112]. Ironically, the abundance of FCDs in optical textures prevented the earlier discovery of N_{TB} since the textures were classified as those of smectics. An excellent illustration of the similarity of FCD-I textures in SmA and N_{TB} and the early history of FCD observations in N_{TB} has been presented by Meyer, Dozov, et al. [113–115]. Dozov and Meyer [113] proposed a coarse-grained theory of N_{TB} using an analogy with the chiral smectic A (SmA*), which is an SmA formed by chiral molecules. An interesting prediction of the theory is that the core of edge dislocations should be extended in the direction perpendicular to the line and to the Burgers vector $\mathbf{b}||\hat{\boldsymbol{\chi}}$. This behavior is opposite to that of edge dislocations in SmA*, in which the core is extended along $\mathbf{b}$. Another interesting prediction is that the line tension of an edge dislocation in N_{TB} is smaller than that of a screw dislocation, which is again a behavior opposite to that of a SmA*. A natural extension of the N_{TB} / SmA* analogy is the prediction of the twist-grain-boundary phase TGB_{TB}, in which blocks of pseudo-lamellar N_{TB} rotate with respect to each other along the direction normal to $\hat{\boldsymbol{\chi}}$; the twist is enabled by lattices of screw dislocations [113]. In both original TGB and TGB_{TB}, the structure is driven by the twist term, but in the original TGB, this twist term originates in the chirality of molecules, while in the TGB_{TB}, the twist is of a structural origin, caused by the

necessity to maintain the constant bend; upon heating, such a phase could melt into an N_U rather than a Ch.

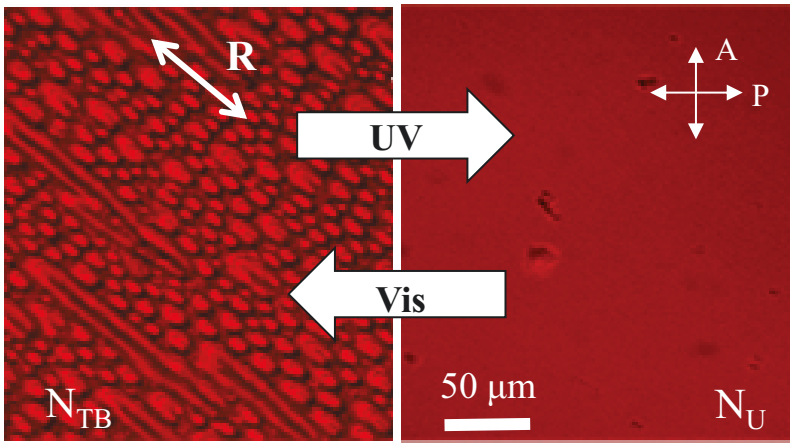

Figure 8:Polarizing optical microscopy textures of CB6OABOBu confined in a 12 µm cell in (a) N_{TB} and (b) N_U. The N_{TB} - N_U transition is caused by UV irradiation; N_{TB} is restored after thermal relaxation or under visible light. The sample is kept at a constant 90°C temperature. R indicates the rubbing direction.

Typically, the FCD-Is are caused by anchoring effects, when the helical axis $\hat{\boldsymbol{\chi}}$ is tangential to at least one of the bounding plates in polygonal textures in flat samples, Figure 7b, and combinations of TFCD and spherical curvatures in freely suspended SmA droplets [102,116]. FCDs form "facets" of SmA nuclei coexisting with the isotropic phase [1,117]. In flat samples with a tangential anchoring at one surface and a homeotropic alignment at another surface (the so-called "hybrid alignment"), FCD-Is degenerate into TFCDs. [10,118] Curved interfaces or the presence of colloidal particles also trigger formations of FCDs [119–122].

FCDs could also be created by applying an electric field [38,103]. The scenario depends on the dielectric anisotropy $\Delta\varepsilon$ of N_{TB} calculated with respect to $\hat{\boldsymbol{\chi}}$. When $\Delta\varepsilon < 0$, TFCDs nucleate when an electric field is applied to a homeotropically aligned N_{TB}, since $\hat{\boldsymbol{\chi}}$ realigns perpendicularly to the field, Figure 9a. The TFCDs then extend into oily streaks of zero or very small Burgers vector (for a detailed description of the geometry of these oily streaks, see Ref.[26]). Each oily streak can be imagined as a cross-section of a TFCD extended along the normal to itself, Figure 9b. The oily streaks reach some maximum width; further extension is impossible because of a finite anchoring at the bounding plates, as explained in detail for a similar scenario in Ch [123]. When the oily streaks fill a substantial area, they relax into square arrays of PFCDs, Figure 9.

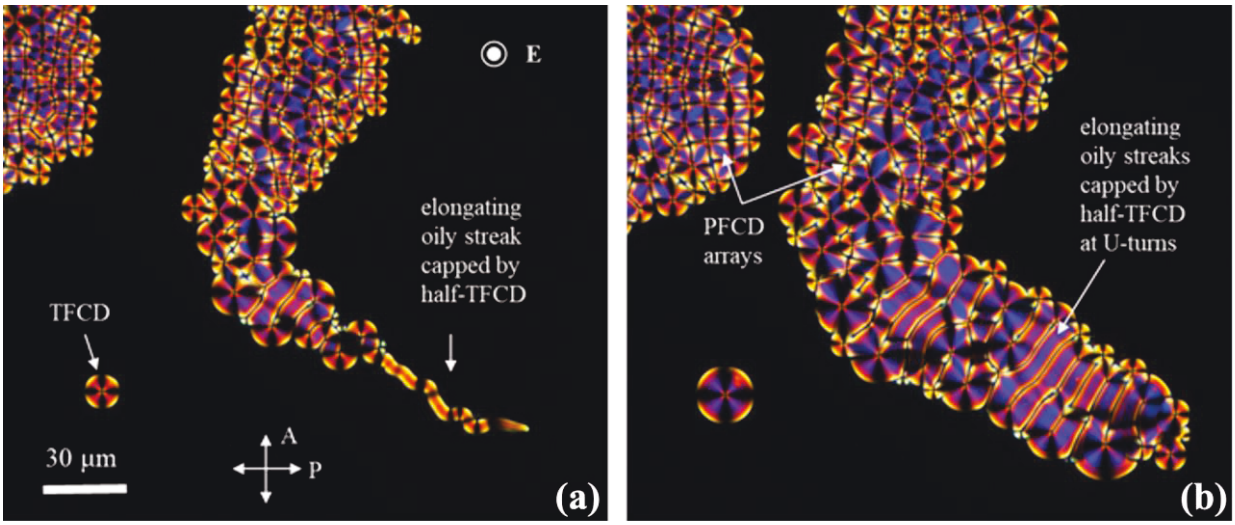

Figure 9: Dynamics of the Frederiks transition from a homeotropic state (extinct regions) to TFCDs, oily streaks, and PFCD by an electric voltage 9 V, 10 kHz, applied normally to the plane of view and to the bounding plates; N_{TB} phase of the mixture DTC5C9:MTC5=60:30 wt % in a cell of thickness 5 μm; $\Delta\varepsilon < 0$; the textures were taken with an interval of 20 s. Nucleating TFCDs elongate into oily streaks of zero Burgers vector; the oily streaks maintain a constant width while elongating and making U-turns; once they fill a substantial area, they transform into PFCD arrays. Materials provided by Vitaly Panov and Georg Mehl. Experiments by Volodymyr Borsh (unpublished).

Krishnamurthy et al. [98] explored the N_{TB} defects in CB7CB, which is of a positive $\Delta\varepsilon$. The electric field was first applied to align $\hat{\boldsymbol{\chi}}$ perpendicularly to the bounding plates. By decreasing the field, one observes scenario similar to that in Figure 9. The TFCDs nucleate, then extend into oily streaks, after which the oily steaks relax into the chains or arrays of TFCDs. The difference between Figure 9 and the textures in Ref. [98] is dictated by different surface anchoring of $\hat{\boldsymbol{\chi}}$ which, in the absence of the field, is normal to the plates in Figure 9 and tangential in Ref. [98]. Because of this, the bases of TFCD and the straight 180° disclinations forming oily streaks are located in the midplane of the sample in Figure 9, while they are at the bounding plates in Ref. [98]. Note also that PFCDs were observed by Pardaev et al. in N_{TB} samples subject to dilations [124].

The instability of TFCDs in N_{TB} and their transformation into PFCDs (and double helices, observed in CB7CB [98] and in other N_{TB}-forming materials [125]) is truly remarkable since from the studies of SmA, it is known that TFCDs could be smoothly embedded into a system of flat parallel layers and thus should not be energetically costly, Figure 7c and Figure 9a. Kleman and Krishnamurthy [16] explained the effect using the so-called extended Volterra process and the

relationship between FCDs and other defects, such as dislocations and disclinations, as described below.

3.4. General properties of FCDs and attached dislocations.

The eccentricity of the ellipse controls an interesting property of FCDs, namely, their relationship with dislocations and disclinations. The necessity of dislocations attached to the ellipse (from outside) is easy to understand by noticing that in Figure 7a, the layers located outside the ellipse should cross the plane of the ellipse at some angle, thus necessitating a grain boundary that could be relaxed by a lattice of edge dislocations if the tilt is not very strong. Figure 10a helps to calculate the sum of Burgers vectors of these dislocations as $b_1 + b_2 = 2a$, where a is the major semi-axis of the ellipse; the minor semi-axis is $b = \sqrt{b_1 b_2}$; the total Burgers vector b_B of dislocations outside the ellipse, relaxing the tilt of the layers above and below the plane of the ellipse is then $b_B = b_1 - b_2 = 4\sqrt{a^2 - b^2} = 4ae$, where $e = \sqrt{1 - \frac{b^2}{a^2}}$ is the eccentricity of the ellipse [11,26]. The last formula suggests that TFCDs do not emit dislocations, which is expected since the TFCD could be smoothly continued by flat parallel layers. However, a non-zero eccentricity implies the existence of dislocations running parallel to the minor axis of the ellipse. The dislocations connecting FCD-Is form grain boundaries [40] and oily streaks observed in many layered mesophases such as the lyotropic lamellar SmA [26] and Ch [123]. Figure 10b,c shows the relationship between FCD-Is of non-zero eccentricity, the tilt of layers in two adjacent domains, and dislocations emitted by the FCD-I. The emitted dislocations might be of various types, with the Burgers vector of each dislocation being equal to the layers' thickness, or they might gather into bundles with giant Burgers vectors, the cores of which split into disclinations [26,123]. In the latter case, often met in lamellar lyotropic, SmA, and Ch phases, the optical contrast of dislocations is high, and they are easily observed under a polarizing optical microscope [26,123].

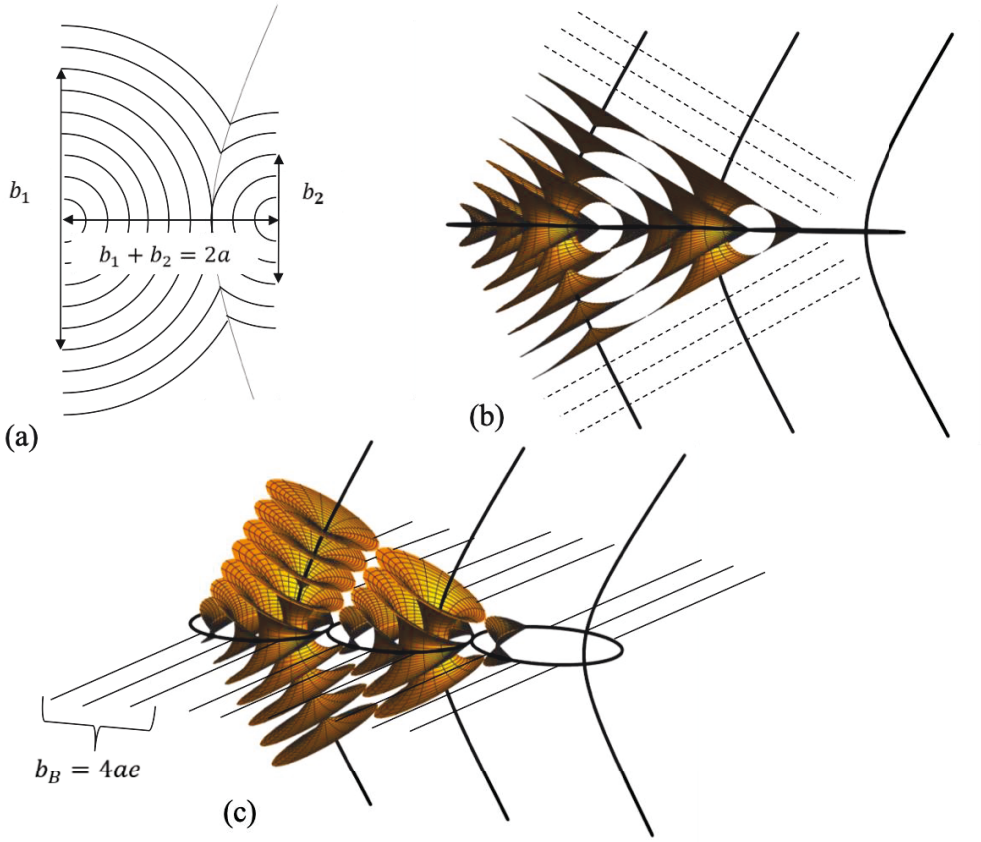

Figure 10: Relationship between FCD-I and dislocations. (a) Cross-section of an FCD-I represented as a pair of dislocations with Burgers vectors b_1 and b_2; (b) FCD-Is relax the grain boundary between two differently tiled systems of layers; (c) the eccentricity e of the ellipses defines the total Burgers vector $b_B = 4ae$ of dislocations emitted by the FCD-I's base.

3.5. FCDs and attached disclinations in N_{TB}.

N_{TB} exhibits a behavior markedly different from the phases mentioned above: the dislocations connecting TFCD-Is produce no detectable optical contrast [16]. Microscopic textures in Figure 7 of Ref. [16] reveal FCD-Is of the eccentricity about 0.7 and the semi-major axis about 10-15 μm. Despite the huge *total* Burgers vector $b_B = 4ae$, expected to be 30-40 μm, these dislocations are not discernable at the background of other textural elements. Kleman and Krishnamurthy suggested that these "invisible" dislocations are either quantized with a small Burgers vectors $2p$ (remember that the period p of N_{TB} is only about 10 nm [74,75]), or are "imperfect" infinitesimal dislocations that relax the structure as scales smaller than p [16]. The necessity to involve disclinations is a more subtle issue rooted in the general concept of the extended Volterra process developed by Kleman and Friedel [11]. In the simplest mesophases,

such as N_U and SmA, the Volterra process is not needed to analyze the properties of defects. However, in more complex structures, one of which is N_{TB}, such a consideration provides a qualitative description of stresses involved and helps to understand textural peculiarities.

The conventional Volterra process consider a *straight* linear defect L as a result of a thought experiment [4] in which (1) one creases a cut surface Σ ending at the defect line L; (2) the two lips Σ^+ and Σ^- of this cut surface are rigidly shifted with respect to each other by some distance $\mathbf{d}(\mathrm{M})$, where M is a point at Σ; Figure 11a illustrates the case when the lips are rotated so that $\mathbf{d}$ increases with the distance from L; (3) the void is filled with a perfectly ordered piece of the material (or, in case of an overlap, a piece of the material is removed); (4) the material is left to relax, which yields the defect L.

The shift of lips $\mathbf{d}(\mathrm{M}) = \mathbf{b} + \mathbf{f} \times \mathbf{OM}$ is generally comprised of a translation $\mathbf{b}$, which is the Burgers vector of the dislocation part of L and a rotation $\mathbf{f} \times \mathbf{OM}$, where $\mathbf{f} = 2\,\boldsymbol{\varpi} \sin\frac{\Omega}{2}$ is the disclination part, called the Frank vector, defined by the angle of rotation Ω and by the unit vector $\boldsymbol{\varpi}$ along the rotation axis; O belongs to the line L and represents the origin of this rotation, Figure 11a. When $\mathbf{b}$ and $\mathbf{f} \times \mathbf{OM}$ are the symmetry elements of the medium, the line L is a *perfect* dislocation or disclinations; when they are not, the line L is an *imperfect* or infinitesimal defect.

The particular geometry in Figure 11a shows a formation of a wedge disclination with $\mathbf{f}$ parallel to L and $\mathbf{b} = 0$. When the medium is positionally ordered, the wedge disclination is accompanied by edge dislocations shown in Figure 11a for a SmA with layers parallel to Σ; these dislocations, with the smallest Burgers vector equal smectic spacing, carry large elastic energy, which typically forbids the entire structure. In N_U, however, the edge dislocations are infinitesimal; the heads of "nails" in Figure 11a could be thought of as the "ends" of the individual molecules; the stresses introduced by L are then viscously relaxed [4].

Consider now a *curved* disclination L. Assume first that the Frank vector $\mathbf{f}$ does not change its orientation and consider two close points O and O′ close to each other, so that $\mathbf{OM} - \mathbf{O'M} = \mathbf{t}\,ds$, where $\mathbf{t}$ is the tangent unit vector to the disclination and ds is the arc length element, Figure 11b. The displacements of lips at a point M viewed from O is $\mathbf{d}(\mathrm{M}) = \mathbf{f} \times \mathbf{OM}$, while it is $\mathbf{d'}(\mathrm{M}) = \mathbf{f} \times \mathbf{O'M}$ when viewed from O′. The difference is non-zero and, importantly, independent of M, yielding a density of infinitesimal dislocations of the Burgers vector $d\mathbf{b} = \mathbf{d'}(\mathrm{M}) - \mathbf{d}(\mathrm{M}) = \mathbf{f} \times (\mathbf{O'M} - \mathbf{OM}) = -\mathbf{f} \times \mathbf{t}\,ds = -2\,\sin\frac{\Omega}{2}(\boldsymbol{\varpi} \times \mathbf{t})ds$, attached to the curved disclination.

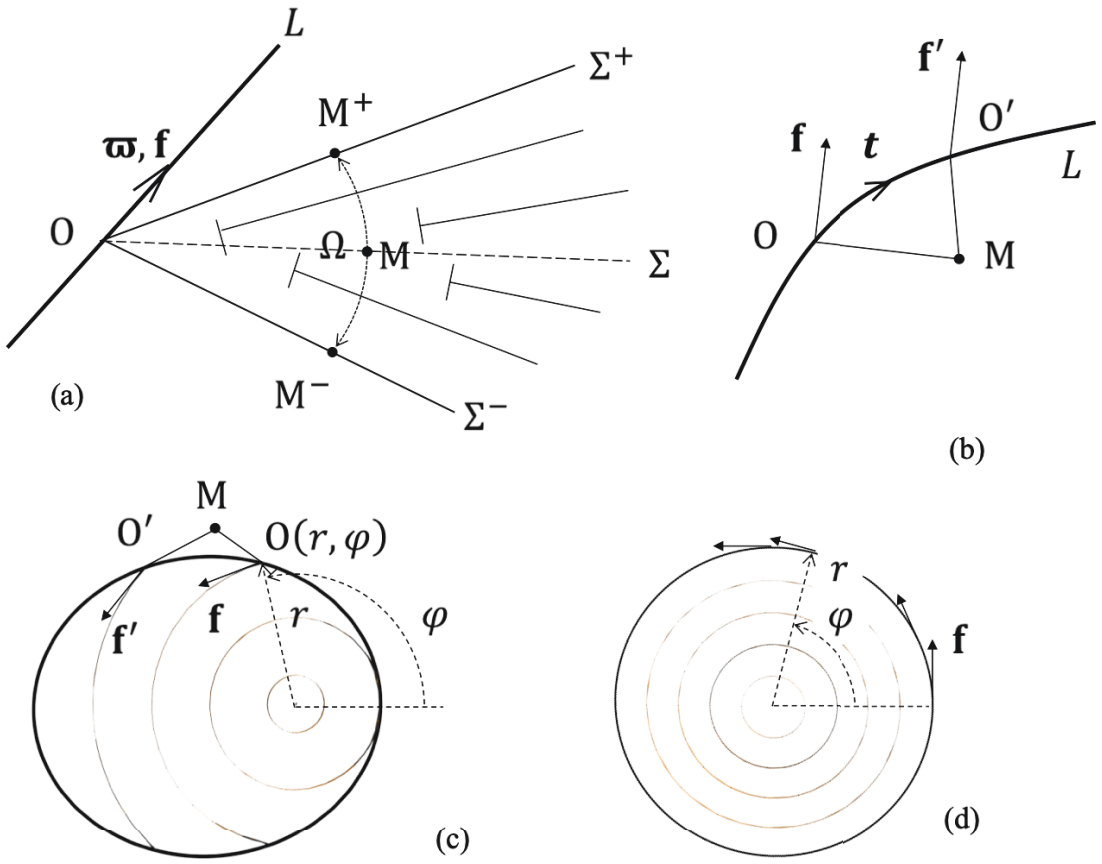

Figure 11: Relationship between FCD-I, TFCD, and disclinations. (a) Volterra process for a straight wedge disclination; (b) a curved disclination emits linear defects; (c) elliptical defect of an FCD-I emits both dislocations and disclinations; (d) circular defect of TFCD emits disclinations; see text.

The ellipse, hyperbola, and parabola of FCDs are all curved disclinations. Moreover, the Frank vector **f** along these lines changes not only the position, as in Figure 11b, but also the orientation, as illustrated in Figure 11c for an ellipse of an FCD-I. The ellipse is topologically equivalent to a wedge disclination loop of a strength $k = \frac{1}{2}$. The Frank vector in the plane of the ellipse is tangent to the layers. When the displacements of a point M is viewed from two close points O and O′, the displacements are not equal: $\mathbf{d}'(\mathrm{M}) = \mathbf{f}' \times \mathbf{O}'\mathbf{M}$ and $\mathbf{d}(\mathrm{M}) = \mathbf{f} \times \mathbf{OM}$; here, $\mathbf{f}' = \mathbf{f} + d\mathbf{f}$ **.** The difference is now $\mathbf{d}'(\mathbf{M}) - \mathbf{d}(\mathrm{M}) = \mathbf{f} \times (\mathbf{O}'\mathbf{M} - \mathbf{OM}) + d\mathbf{f} \times \mathbf{OM} = -\mathbf{f} \times \mathbf{t}\ ds + d\mathbf{f} \times \mathbf{OM}$ and represents the sum of dislocations of the Burgers vector $d\mathbf{b} = -\mathbf{f} \times \mathbf{t}\, ds$ and disclinations of the Frank vector $d\mathbf{f}$, all attached to the ellipse between the points O and O′. In a SmA, any direction

within the smectic layer is a two-fold symmetry axis, thus **f** could assume any orientation within the layer. In N_{TB}, Figure 5, the only twofold symmetry axis is along a vector $\hat{\boldsymbol{\tau}}$, which is normal to the local director and the helicoidal axis $\hat{\boldsymbol{\chi}}$; thus **f** should be parallel to $\hat{\boldsymbol{\tau}}$ and $d\mathbf{f}$ is along the normal $\hat{\boldsymbol{\chi}}$ to the layers.

Therefore, curved disclination with a variable Frank vector must emit both dislocations and disclinations. When the ellipse is a circle, the dislocations are absent, but the attached disclinations persist. The Frank vector around the circular wedge loop is rotating, $\mathbf{f} = 2\ \sin\frac{\Omega}{2}(-\sin\varphi, \cos\varphi)$, where φ is the polar angle defined in Figure 11d. Since the circular defect is a wedge disclination of the strength $k = \frac{1}{2}$, the rotation angle Ω of the two lips of the Volterra cut is π. Then the density of attached disclinations $\left|\frac{d\mathbf{f}}{ds}\right| = \left|-\frac{2}{r}(\cos\varphi, \sin\varphi)\right| = \frac{2}{r}$ [16].

In SmA, these infinitesimal disclinations are fully relaxed since the molecular structure is rotationally symmetric around the normal to the layers. When the layers show some in-plane ordering, which is the case of SmC, SmC*, biaxial SmA, Ch, and N_{TB}, this relaxation is not possible. For example, it is well known that the FCD-Is in SmC [71,126,127] and SmC* [34] show two disclinations of strength $k = -1$ each connecting the ellipse to the hyperbola. TFCDs in a biaxial SmA, show disclinations with a variety of strengths, including $k = -\frac{1}{2}$ and $k = -1$, depending on the geometry of the secondary director field outside the TFCD [106]. In N_{TB}, these disclinations might be either perfect with a well-defined strength or infinitesimal. In either case, they are hard to observe, mostly because of a very narrow core, the extension of which should be comparable to the pitch, i.e., only about 10 nm.

In contrast to the circular wedge disclination of strength $k = \frac{1}{2}$, the two parabolas of a PFCD, Figure 7d, as well as the hyperbola of an FCD-I, Figure 7a,b, and the straight defect line of a TFCD, Figure 7c, are all of a strength $k = 1$, since the normal $\hat{\boldsymbol{\chi}}$ to the layers wraps around these defects on a full conical surface. Therefore, these defects do not omit disclinations (nor dislocations). Kleman and Krishnamurthy suggested that this difference between the circular disclinations in TFCD and two parabolic disclinations in N_{TB} is responsible for the instability of TFCDs and their replacement by PFCDs [16]. The detailed molecular arrangements associated with heliconical N_{TB} trihedron in FCDs are hard to establish because of the smallness of the pitch

as compared to the typical extension of FCDs; this problem might eventually be solved by numerical simulations.

Binysh, Pollard, and Alexander [128] made a step forward in deciphering the structure of linear defects and associated textures such as PFCDs in N_{TB} by considering line defects along which bend, defined as $\mathbf{B} = \hat{\mathbf{n}} \times \mathrm{curl}\hat{\mathbf{n}}$, vanishes. One example are wedge disclinations and edge dislocations of strength k, described by the director field $\hat{\mathbf{n}} = (\sin\theta\cos\varphi, \sin\theta\sin\varphi, \cos\theta)$. For a disclination, the phase is $\varphi = qz + k\,\mathrm{artan}(y/x)$, while the conical angle θ decreases from its equilibrium bulk value far away from the defect to 0 at the core; at the core, the director line is straight and parallel to the rotation axis. In the edge dislocation, $\varphi = qz + k\,\mathrm{artan}(z/x)$.

PFCDs in N_{TB} textures are accompanied by a macroscopic electric polarization due to the curvature of layers, as discovered by Pardaev et al. [124]. Analysis by second harmonic generation light scattering demonstrates that the polarization vector is in the plane normal to the axis of twofold symmetry of the PFCD; its existence is associated with the strong deformations at the cusps of the Dupin cyclides.

3.6. Droplets of N_{TB}.

Droplets of liquid crystals suspended in an immiscible fluid [92,129–133] or emerging in biphasic coexistence [99,134,135] show fascinating inner structures thanks to their non-zero Euler characteristic, $E = 2$ [131–133]. Droplets produce intriguing phenomena such as the Lehmann effect [136], spontaneous division during phase transitions [137], and demonstrate a potential for applications in optics, photonics [138,139], and sensing [140]. According to the Gauss-Bonet theorem, a vector field defined at a spherical surface must feature topological defects of a total strength equal E. Topological defects that satisfy the theorem by the lowest possible value of the net topological charges are in the state of thermodynamic equilibrium. In layered liquid crystals, surface anchoring often requires the layers to be tangential to the interface. If there is a vector order parameter within the layers, this packing results in two disclinations of strength $k = 1$ or one disclination of strength $k = 2$ [4,71]; the latter resembles the Dirac monopole [70], as already alluded to. In Ch, the structure is known as the Frank-Pryce configuration [141,142]. As a rule, one observes one disclination of a strength $k = 2$ and sometimes two disclinations of a strength $k = 1$ each [133,143,144]. Numerical simulations by Seč et al. [145] demonstrate that the structure with $k = 2$ is energetically preferable for a sufficient droplet diameter-to-pitch ratio.

Freely suspended spherical N_{TB} droplets have been studied only recently [92,99,135]. Eremin et al. [92,146] observed stripes at the droplets' surface, which were attributed to the surface anchoring effect and formation of an analog of a "fingerprint" texture known in Ch, which is formed when the helicoidal axis is tangential to the interface. Textures in Fig.10 of Ref. [92] do show radial lines that might be related to the $k = 2$ disclinations of the Frank-Pryce structure or to the axial defect of a TFCD embedded into the concentric packing of N_{TB} pseudolayers [102]; however, the analysis in Ref. [92] concluded that these lines represent "U-turns" of folded phesudolayers.

An evidence of the Frank-Pryce structure with a radial $k = 2$ disclination was presented by Krishnamurthy et al. [99] in elegant experiments in which the N_{TB} droplets were formed in the biphasic N_U-N_{TB} region. The $\hat{\boldsymbol{\chi}}$-axis of an N_{TB} droplet arranges into a radial point defect-hedgehog, being perpendicular to the N_{TB}-N_U interface. The radial defects are more prominent in small droplets (10-20 μm) than in larger ones. As the droplets become larger and touches the bounding plates, the Frank-Pryce structure changes completely, by splitting the central radial point defect into an extended loop with a thick core and a complicated structure. The most recent study of N_{TB} droplets [135] explored the fact that the surrounding N phase forms a hyperbolic hedgehog so that the N_{TB} droplet together with a satellite hedgehog is of dipolar symmetry. Because of this symmetry, the droplets could be transported by an applied electric field, which interacts with the N_U director through dielectric and flexoelectric mechanisms [135], similarly to the electrophoresis of colloidal particles in N_U [147].

The structure of the N_{TB} defects was also studied in lens-shaped sessile droplets of a photoresponsive flexible dimer by Yoshioka et al. [148] In contrast to the majority of conventional calamitic N materials, the LC–air interface of the present dimer nematic imposes a planar anchoring. Geometry-dictated competition of this anchoring at the curved LC-air interface with the substrate anchoring, together with the elastic anisotropy of N_{TB} induces unique frustrations in the structure of the droplets. It was found that large N_{TB} droplets residing at a plate with a homeotropic alignment have different structures in the inner and outer regions, Figure 12a. The striped texture of the outer region can result from the N_{TB} pseudo-layer structure. N_{TB} droplets at planar substrates show stripes decorated with zigzag undulations, Figure 12b. Such stripes and undulations are often observed in SmA shells [149,150] and, as already stated, in N_{TB} planar cells

[88,111,151]. The pseudo-layered structure of N_{TB} buckles in response to the constraints imposed by the curved surface and by shrinkage of layers upon cooling, Figure 12c.

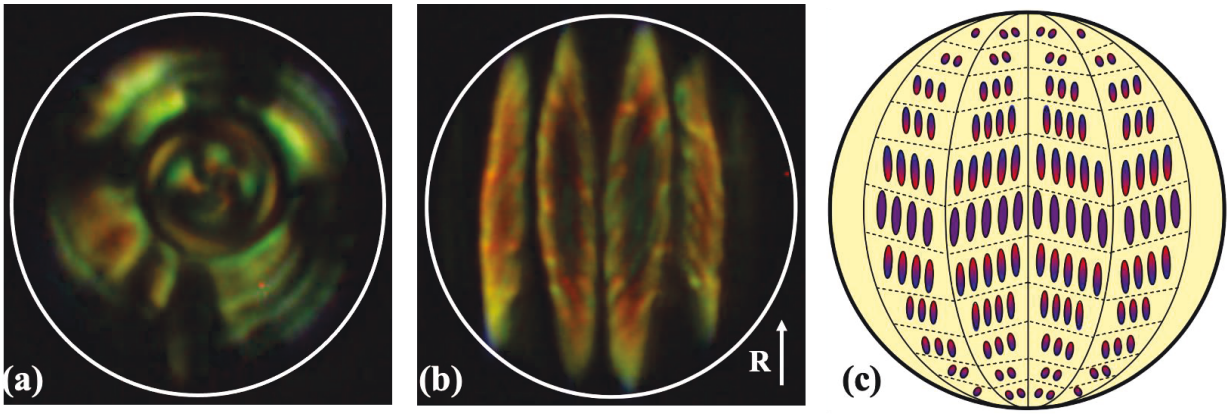

Figure 12: Polarization micrograph of spherical-cap droplets in the N_{TB} phase placed (a) at a plate with a homeotropic anchoring and (b) at a plate with unidirectionally planar alignment along the vertical direction. (c) Model (borrowed from [150]*) for the stripe domains of the sessile N_{TB} droplets on the planar substrate. In this model, the pseudo-layered nature of N_{TB} is the cause of the stripes and undulations. Dotted lines show the direction of the pseudo-layers. The ellipses show the point-by-point distributions of the N directors projected onto the plane. Dashed layers indicate the projection of the pseudo layers toward the plane and look thinner near the poles due to the larger tilt with respect to the plane.*

4. DEFECT-MEDIATED PHASES OF BENT-CORE LIQUID CRYSTALS

In liquid crystals, defects often correspond to the ground state of the system. A simple example is a spherical N droplet that carries either two-point defects at the poles or one point defect in the bulk, depending on whether the surface anchoring is tangential or perpendicular. The energy minimum is achieved by balancing the surface anchoring and bulk elastic energy (the surface tension term in thermotropic LCs is often much larger than the other two terms, which explains the nearly spherical shape of the drops). There are also cases when the defects occur to relieve internal frustrations in the bulk, in which case they are an intrinsic part of the structural organization of the mesophase.

A well-known example are the blue phases (BP) that appear between the isotropic and cholesteric phase. They often exhibit a submicron scale twist and show selective reflection in the visible range. The first examples observed by Reinitzer [152], Lehman [153], Friedel [1], then by Gray [154] showed blue color (hence the name). In addition to the structural color, it was also shown that the

BP phase has no birefringence, but is optically active, indicating chiral, deformable structure of high symmetry. Based on this, without much experimental details, it was already suggested in 1969 by Saupe [155] that the blue phase has a periodic structure formed by cylindrically symmetric local director configuration in which the preferred orientation rotates along all directions perpendicular to the symmetry axis. The local configuration corresponds to a doubly twisted cylinder, where at the edge of the cylinders the director is twisted with respect to that of the core. The idea eventually led to the modern understanding of blue phases as packings of cylinders with double twist. Chiral interactions of molecules favor the double twist as opposed to the one-directional twist. However, as one moves away from the axis of the cylinder, the double twist is gradually transforming into a one-directional twist with a reduction of the energy gain. The radius of the cylinder is thus limited, typically by a length scale comparable to the half-pitch. The finite-size cylinders could not tile space continuously. The frustration between the local double twists and continuous tiling is resolved by a lattice of disclinations that form at the junctions of the cylinders [156–158]. These disclinations could be distributed regularly or irregularly, forming various subclasses of the blue phases. Similar structures could also be observed in smectic materials [159].

Chiral mixtures of rod-like and bent-core molecules often produce blue phases with an extended range of the thermodynamic stability blue phase II (BPII) has been prepared [160] and its electrooptical performance has been evaluated. A broad (>20°C) range BPIII phase showing electrooptical switching in a few tens of milliseconds was obtained by Taushanoff et al by adding a few percentages of chiral dopant to achiral bent-core nematics. [161] It was proposed that broad-temperature range smectic nanoclusters inhibit the long-range order of the double twisted helical structures and stabilize the amorphous BPIII phase.

Another example of frustrated mesophases with defects is the twist-grain boundary smectic A phase (TGBA*) predicted theoretically by Renn and Lubensky [162]. The model is based on the analogy between smectics and superconductors proposed by de Gennes. [163] The TGBA* phase was experimentally observed by Goodby et al. [164] In TGBA*, the frustration is between the chiral interactions and the tendency of smectic layers to preserve equidistance. The frustration is resolved by introducing twist grain boundaries comprised of screw dislocations that separate blocks of smectic ordering, allowing them to twist with respect to each other. The phase is stable,

because the increase in the free energy due to the introduction of the grain boundaries is less than the decrease of free energy due to the director twist. The pitch p of the TGB phase is determined by the distance between grains l and the rotation angle α of the director in crossing a grain boundary, as $p = 2\pi l/\alpha$. For example, if l=25 nm and $\alpha=\pi/9$, then p=450 nm.

Bent-core liquid crystals exhibit an even richer variety of defect-mediated phases than calamitic LCs. Some of them (possible TGB phases and broad temperature range blue phases) result from the intrinsic molecular chirality induced by chiral dopants, or chiral stereo center built in the bent-core molecules, while the twist-bend modulated smectic phase, dark conglomerate (DC) phase, helical nanofilament (HNF a.k.a. B_4) phase and polarization modulated (a.k.a. B_7) phase are triggered by the spontaneous chiral symmetry breaking in achiral systems.

4.1. Chiral N_{TB} - possible TGB_{TB} phase

One of the interesting questions related to bent-shaped materials is how the structural chirality of the N_{TB} phase responds to the presence of molecular chirality. The effect of the chiral additive on the N_{TB} structure is of interest to the entire liquid crystal science since it represents an interaction between molecular chirality and spontaneous chiral symmetry breaking with ambidextrous nanoscale chirality. It has been studied theoretically by Longa et al. [165,166] using a Landau-de Gennes theory of N_{TB}, supplemented by a term representing intrinsic molecular chirality. Besides $N^*$and N^*_{TB}, the model also predicts a globally polar and chiral twist-bend nematic N^*_{TBp} with a periodicity of the director field comparable to that of the N^* phase.

A natural extension of the N_{TB} / SmA* analogy is the already mentioned prediction by Dozov and Meyer [113] of the twist-grain-boundary phase TGB_{TB}, in which blocks of pseudo-lamellar N_{TB} rotate with respect to each other along the direction normal to $\hat{\boldsymbol{\chi}}$; the twist is enabled by lattices of screw dislocations. In both original TGBA* and TGB_{TB}, the structure is driven by the twist term, but in the original TGBA*, this twist term originates in the chirality of molecules, while in the TGB_{TB}, the twist is of a structural origin, caused by the necessity to maintain the constant bend; upon heating, such a phase could melt into an N_U rather than a Ch.

The first experimental observations of the effect of molecular chirality on the structure of flexibly bent dimeric molecules showed that the helical pitch becomes distorted [167] or is even unwound

[168], in the chiral N_{TB} (N^*_{TB}) phase. Gorecka et al [169] found direct transition between the N^* and N^*_{TB} phases for asymmetric bi-mesogens in which rod-like units are connected with a cholesteric unit, whereas mixing chiral moiety to a symmetric achiral bent-shape dimer (CB6OCB), Walker et al [170] found an intermediate phase with square lattice between the N^* and N^*_{TB} phases. Such a structure was attributed to the low bend elastic constant in the bottom of the N^* phase.[171] Walker et al [170] also described the first examples of the N^*_{TB} phase formed by H-bonded donors and acceptors. The properties of this N^*_{TB} material strongly resemble those previously observed in covalently bonded materials. The temperature range of N^*_{TB} is wider than that of the conventional N_{TB} phase exhibited by achiral materials; upon cooling, N^*_{TB} transitions into a SmC^*. [172] Using chiral additive with very high helical twisting power, the existence of a novel N^*_X phase was reported also at the temperatures below the N^*_{TB} phase. [173]

Using resonant soft x-ray, induced circular dichroism and several optical microscopy experimental techniques, Murachver et al reported the first quantitative results on the effect of chiral additives on the nanostructure of a room temperature mixture of LC dimers abbreviated KA0.2. [174] They found that while the chiral additive causes the micron-scale pitch of the dopant-induced helical structure to decrease with increasing dopant concentration in the N^* phase, in the N^*_{TB} phase both the micron-scale helical pitch and the nanoscale pitch of the ambidextrous spontaneous heliconical structure are increasing. At concentrations c≥2wt% of a chiral dopant, a new phase, resembling TGBA* and termed TGB_{TB} phase, appears between the N^* and N^*_{TB} phases. Such a phase is plausible since the N_{TB} phase formed by flexibly bent-shape molecules has a pseudo-layer structure due to the nanoscale helix, therefore, like the TGBA* phase of layered SmA phase, the addition of chiral dopant may lead to twist-grain boundary phase. The illustration of the structures of the N^*, N^*_{TB} and the proposed TGB_{TB} phases are shown in Figure 13.

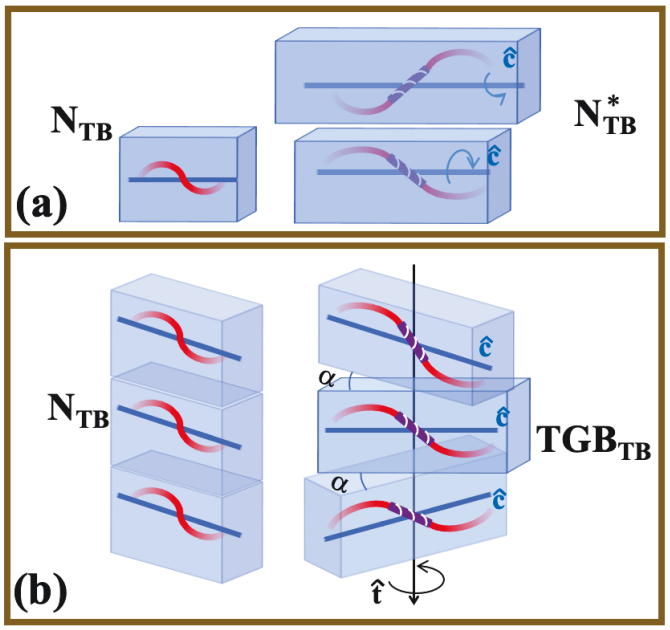

Figure 13: Schematic illustration of chirality transfers due to chiral additives (purple rod with white grooves to illustrate molecular chirality) in the N and N_{TB} phase. (a) Chiral additives in the N_{TB} phase, the molecular chirality may modulate the nanoscale pitch, or (c) it can break the pseudo layers into blocks that rotate with respect to each other (TGB_{TB}).

4.2. Dark Conglomerate phase

The dark conglomerate (DC) phases, as the name indicates, are optically isotropic phases that exhibit conglomerates of macroscopic chiral domains. The internal structure consists of polar smectic layers with relatively short interlayer correlation length. Freeze-fracture TEM images revealed that in the DC, although the local layering is well defined, the layer topography is highly curved, forming saddle-shaped domains. [107] The in-layer frustration, caused by orthogonal tilting of the molecular segments in the upper and lower halves of each smectic layer, can be relieved by saddle-splay curvature. As a result, the DC structure is a 3D mesh of saddle-splay domains with significant negative Gaussian curvature of the smectic layers, Figure 14. Freeze-fracture TEM textures reveal edges of saddle-shaped layers [red arrow, Figure 14a; magnified in Figure 14b] involved in the formation of the mesh. The thermotropic DC phase resembles the sponge L_3 phase in lyotropic lamellar phases formed by wedge-shaped amphiphilic molecules [175].

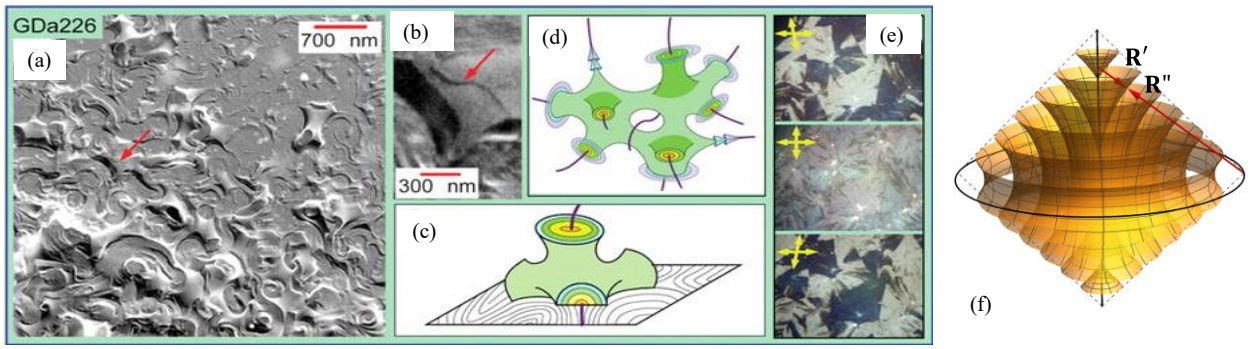

Figure 14: Freeze-fracture TEM (a and b) and polarized optical microscopy images (e) of DC phase formed by a (c,d) mesh of saddle-splayed domains, (f) modelled as conically-limited TFCDs with radii of curvature R' and R" of opposite signs. Parts a-e are reproduced from Ref. [102] with permission.

The microscopic textures of the DC phases appear dark under crossed polarizers, because the birefringent regions are oriented randomly at sub-micron length scale, middle image of Figure 14e. [176] The phase exhibits chiral domains of opposite handedness, which are readily revealed by the circular dichroism in observations with uncrossed polarizers, top and bottom images of Figure 14e. A sufficiently high electric field transforms the sponge structure into a highly birefringent texture [177–180] with a synclinic and ferroelectric order (SmC_SP_F) that has long-range interlayer correlations.

The DC structure with local saddle-splay deformations of layers could be modelled as a 3D mesh of interconnected TFCDs, Figure 14c,d,f. Each TFCD is constructed by a family of parallel saddle-splay smectic layers with negative Gaussian curvature wrapped around a circular base and a central axis passing through the circle's center, Figure 14f. The normals to the layers are straight lines connecting the circle to the axis. The domain is limited by two conical surfaces which facilitate tiling of space with differently oriented TFCDs. Observe the difference with the TFCDs limited by circular cylindrical surfaces, Figure 7c, which could be smoothly embedded into a stack of flat parallel layers, a common feature of textures in conventional smectics and N_{TB}, Figure 9. The saddle-splay is not compatible with a long-range positional order and could be realized only locally. The free energy density depends on principal curvatures $\sigma' = 1/R'$ and $\sigma'' = 1/R"$, where R' and $R"$ are the principal radii of curvature of opposite signs, depicted in Figure 14f [102]:

$$f = \frac{1}{2}K(\sigma' + \sigma'')^2 + \bar{K}\sigma'\sigma'' + G(\sigma' - \sigma''), \qquad (1)$$

where $K > 0$ and $G > 0$, but $\bar{K} < 0$ to penalize pure saddle splay. The combination of the mean curvature K term and the Gaussian $\bar{K}$-term favors flat layers, while the saddle-splay deformations are driven by the last G-term; this term reflects the tendency of layers to twist along the polarization direction which is in the plane of the layers. Using the analytical expressions for σ' and σ'' within a TFCD [4,41], Hough et al [107] demonstrated that the saddle-splay structure is energetically preferable than flat layers if the typical radius and height of the domain is $a \sim 10d(1 - 3K/\bar{K})$, where $d = 4$ nm is the smectic layer thickness. Assuming $K/\bar{K} \sim -1$, the result a~200 nm is consistent with the observed structure, Figure 14a.

4.3. Helical Nanofilament Phase (HNF).

Another intriguing bent-shaped LC defect phase with a 3D nanostructure is the Helical Nanofilament (HNF) phase (a.k.a. B_4 phase). FFTEM studies of the HNF phase revealed an assembly of twisted layers stacked to form chiral nano-bundles of a width *w*~40nm and pitch *p*~200 nm. [181,182]

As in the case of DC, the hierarchical self-assembly of HNF originates from the shape of the bent-core molecules that form well-defined smectic layers with in-plane order, macroscopic polarization, and tilt of the molecular planes, which makes the individual layers chiral. A crucial feature is that tilts of the upper and lower halves of the bent-core molecules are not coplanar. This mismatch between the top and bottom halves of the smectic layers is relieved by their local saddle-splay deformations. HNFs are immensely attractive for photovoltaic and chiral separation applications and as templates for the chiral spatial assembly of guest molecules [183].

The individual HNF has been modeled as a bundle of twisted ribbons , Figure 15a. [181]. Within the bundle, the central smectic layer is a minimal surface. The free energy density, given again by Eq.(1), is reduced to a particularly simple form $f = -\bar{K}\sigma^2 + 2G\sigma$ for this minimal surface, as $\sigma' = -\sigma'' = \sigma$. Minimization suggests that the preferred curvature is $\sigma_P = G/\bar{K}$, which relates the pitch to the elastic moduli, $p = 2\pi/\sigma_P = 2\pi\bar{K}/G$.

Matsumoto et al. [184] demonstrated that the twisted bundles of smectic layers, Figure 15b, could be obtained by minimizing the Landau-de Gennes free energy of a SmA comprised of chiral molecules. The solution is a local phase field that can be expressed in cylindrical coordinates as $\phi^{loc} = rcos(q_o z - \theta)$, where $\theta = (q_o z, q_o z + \pi)$ is the two-dimensional surface of a helicoid.

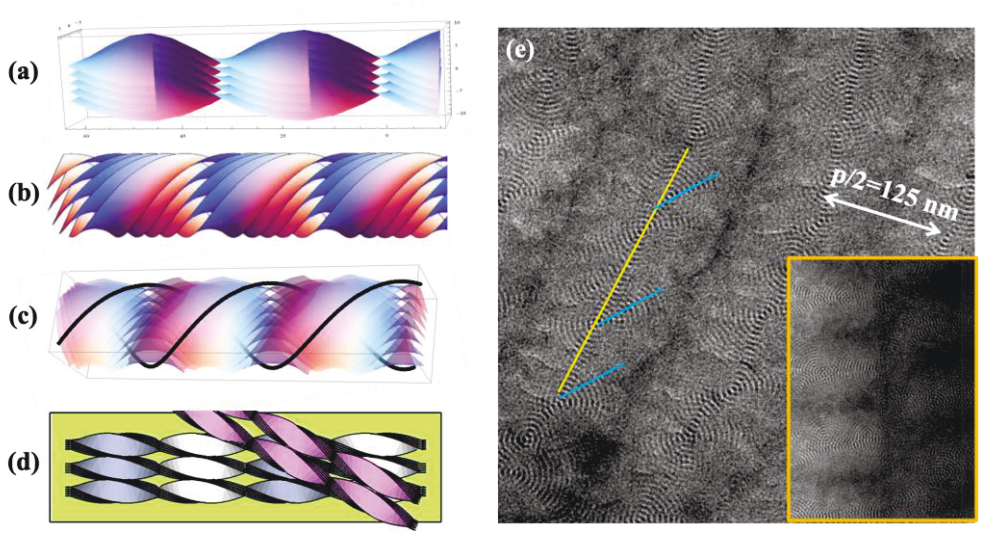

Figure 15: Models and Transmission Electron Microscopy (TEM) images of helical nanofilaments (HNF). (a) Model proposed by Hough et al. [181]*; (b) Model proposed by Matsumoto et al.* [184]*. (c) Model of giant screw dislocation corresponding to the TEM image in the inset of (e). (d) Illustration of the overlapping helical filaments corresponding the TEM image shown in (e).*

Freeze Fracture Transmission Electron Microscopy (FFTEM) studies show that the HNF organization is fragile and transforms into focal conic domains near a glass substrate [185]. Cryo-TEM studies on the prototype HNF materials, phenylene bis(alkoxyphenyliminomethyl) benzoate series, PnOPIMB [186,187] with n= 7, 8, 9 and 12 carbons in their alkyloxy tails, show stripes parallel to the filament axis separated periodically by distances corresponding to half of the pitch, as seen in Figure 15e. Such a structure agrees with the model in Figure 15b.

Some HNF textures reveal screw dislocations of a giant Burgers vector [12,188], see inset in Figure 15e. These giant screw dislocations were demonstrated by Kleman [3,4] to split into two intertwined disclinations of strength $k = 1/2$ that wrap around a cylindrical surface containing nested helicoidal smectic layers, Figure 15c. The period p of the helicoidal disclinations equals the Burgers vector b. It is usually on the scales of tens of micrometers, orders of magnitude larger than the nanometer thickness of smectic layers. The model, proposed in 1977 [3,4], explained peculiar "double helices" textures of thick slabs of SmA [189]. Its construction is explained in the next subsection, in which we discuss supramicron-scale helical ribbons in the B_7 phase. Remarkably, the Kleman's model, derived from geometrical and elastic properties of screw dislocations in SmA, is practically identical to the HNF models of Hough et al. [181] and Matsumoto et al. [184], compare Figure 15c to Figure 15a,b.

Sufficiently thick films of n=8,9 homologs exhibit nanofilament layers stacking on top of each other in a twisted fashion, with the twist angle about 40° between subsequent layers. The structure thus features a double twist of a type different from the one in blue phases. One axis of the twist is along the axis of each nanofilament; the orthogonal second axis of twist is associated with the rotation of nanofilament layers. This double twisted structure explains both the observed structural blue color of some HNF materials and their ambidextrous optical activity. [190] A sketch of this arrangement is shown in Figure 15d where the filaments running in different directions are shown by yellow and light blue lines. Figure 15e shows the corresponding TEM texture of a film with two layers of twisted filaments.

HNFs made from achiral bent-shape molecules are macroscopically racemic consisting of left and right-handed homochiral domains. HNFs containing chiral dopants or formed by chiral molecules [191,192] are either homochiral or diastereomeric with unequal amounts of left and right-handed HNF nucleation [193].

Modulated helical nanofilament phases (HNF_{mod} and HNF_{mod2}), characterized by an additional 1D and 2D in-layer modulations were recently found as well. [194,195] The handedness of the resulting HNF_{mod2} phase is controlled by the longer arm of the nonsymmetric bent-core molecules. [196] Heliconical-layered nanocylinders composed of up to 10 coaxial heliconical layers, which can split or merge, braid, and self-assemble into a variety of modes including feather- or herringbone-type structures, concentric rings, or hollow nest-like superstructures were also found for a class of tris-biphenyl bent-core molecules with a single chiral side chain in the longer para-side of the molecule. These multi-level hierarchical self-assembled structures, rivaling muscle fibers, display blue structural color and show immense structural and morphological complexity. [197]

4.4. B_7 textures

Bent core materials with bulky molecular moieties such as NO_2 in their central benzene ring [198,199] form peculiar micrometer-scale helical patterns and freely suspended filaments [200–205]. Although the textures observed upon moderate-rate (<1C/min) cooling from the isotropic phase are very complicated (see Figure 16a,b), all of these structures contain some periodicity comparable to the film thickness. [198]

Interestingly, under very slow cooling (~1°C/hour), the stripes become oriented uniformly over large (mm-size) areas, Figure 16(c,d). [206] These textures can be understood as parallel arrays of coaxial layers separated by periodic defects as illustrated in Figure 16(d). Before their nanostructure was understood, these textures were labeled as B_7 phase.

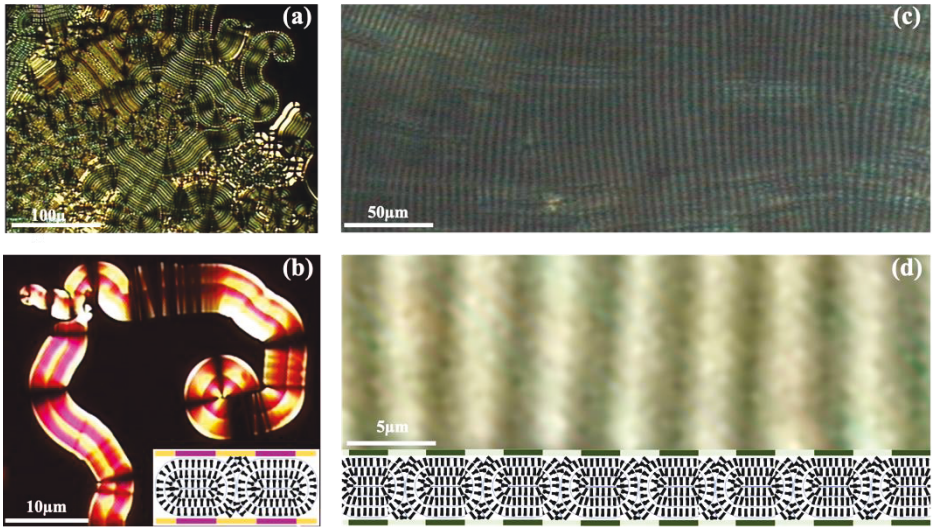

Figure 16: Typical peculiar textures seen in polarizing microscope when bent-core materials are cooled from the isotropic (black background) to the B_7 textures. (a) and (b) Cooling rate: 1°C/min. (c) and (d) Stripe texture formed after very slow (8mK/min) cooling. (c) shows a larger area, while (d) represents a small area with the proposed layer structure.

The amazing optical B_7 textures attracted intense research interest [58,198,212,213,199,200,204,207–211]. An extensive study by Nastishin et al. [188] revealed that upon fast cooling from an isotropic phase, B_7 phase of a material D14F3 formed by achiral molecules nucleates as individual helicoidal ribbons (HRs) of both handednesses. The pitch p is on the order of tens of micrometers, Figure 17a,b, much larger than the 200 nm pitch of similar formations in the HNF phases. There are two types of the HRs, called respectively slim (S) and fat (F) filaments because of the difference in their width w, Figure 17a,b. The HRs show a pronounced unidirectional growth along their axis. Nucleating ribbons quickly elongate until they reach the sample's boundaries or other nuclei.

To explain the HRs, Kleman and co-workers considered B_7 phase as being formed by smectic layers with an in-layer periodic 1D modulation, the direction of which rotates helically from one smectic layer to the next . [12,188] This B_7 ordering is called "lamello-columnar", the "columns" being the elements of modulation. The question is whether the lamello-columnar structures with

helicoidally twisted modulations could be deformed while remaining isometric, i.e., preserving the parallelism of layers and equidistance of modulations. The answer is affirmative, if the structure represents nested helicoidal layers [12,188].

The nucleating HR of B_7, according to Refs. [12,188], is built around a parental central smectic layer in the form of a ruled helicoid, generated by a straight line perpendicular to the helical axis and rotating with a pitch p about it, Figure 17c. The parental helicoid is a minimal surface with a vanishing mean curvature $\sigma' + \sigma'' = 0$. The adjacent smectic layers are shifted along the normal to the axis, forming a bundle of parallel nested helicoids, Figure 17d. The focal surfaces of these nested helicoids form two intertwined $k = 1/2$ disclinations twisted around each other on a cylindrical surface of a diameter $w = p/\pi$. Up to this point, the construction is the same as for a screw dislocation of a giant Burgers vector $b = p$ [3,4]. What makes it applicable to the lamello-columnar structure of B_7 is that the "columns" within the smectic layers, represented by helicoidal lines in Figure 17d wrapping around the central axis, preserve their equidistance. These columnar modulations experience a helical twist from one layer to the next. Since the twist extends radially from the HR axis, it is a double-twist, similar to the double twist of the director in blue phases. In a particular ribbon, the twist is either left-handed or right-handed, as expected because of achiral nature of the molecules.

The model imposes a strict relationship between the pitch and the diameter of the HR, $p = \pi w$, which is very close to what is the observed experimentally for slim filaments [188]. It also supports the experimental observation of the fast unidirectional growth. The unidirectional character of the growth of HRs is distinctively different from the multidirectional growth of smectics growing from their melt in form of bâttonets [1,4,8,117]. HR nuclei, meeting on their growth, do not coalesce, remaining mutually impenetrable. This steric interaction suggests that the HRs have well-defined geometric boundaries, beyond which they cannot extend and within which any distortion increases the energy. The behavior is akin to that of impenetrable FCDs [4].

On slow cooling, the HRs nucleate together with non-helical objects with the geometry of developable domains (DDs), common in columnar phases with 2D translational order. When a sample is allowed to anneal at a fixed temperature, the HRs show their metastable nature, transforming into non-helical DDs. [191]

One peculiar shape is a DD built around a point defect, Figure 18a, theoretically predicted by Kleman [43] for columnar phases. The Kleman singular point DD is limited by a sphere and a double cone with its apex at the sphere's center, Figure 18b. Parallel bent columns are packed on concentric equidistant spheres. Each column starts at the surface of one cone, runs along a 3D curve along the surface of a given sphere and ends at the other cone. Other columns are obtained by axial rotations. The 2D translational order is preserved at the planes perpendicular to the columns. Although the bent columns are wound along the spheres, forming a chiral (left or right) structure, the system of parallel columns does not suffer twist ($\hat{\mathbf{n}}\mathrm{curl}\hat{\mathbf{n}} = 0$) nor splay ($\mathrm{div}\hat{\mathbf{n}} = \mathbf{0}$). The only orientational deformation is the bend $\hat{\mathbf{n}} \times \mathrm{curl}\hat{\mathbf{n}}$ of the columns.

Interestingly, the bent-core materials with HR nucleation from the isotropic phase, can be pulled into smooth cylindrical filaments suspended in air. [200] These filaments are very similar to those found in columnar LCs [214] further enforcing the lamello-columnar structure proposed by Kleman et al. [12,188].

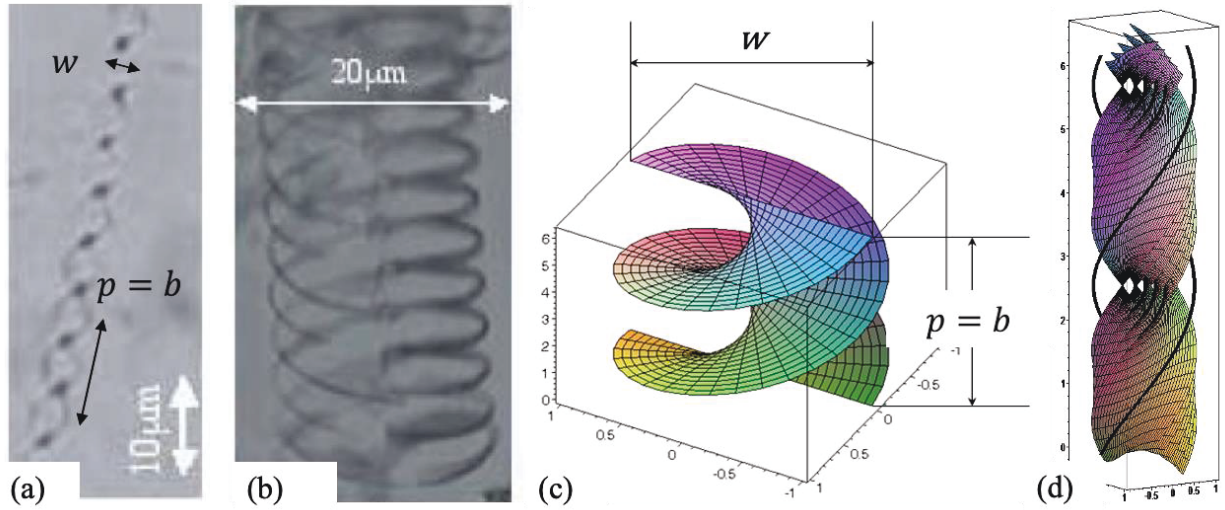

Figure 17: (a) Slim and (b) fat helical ribbons (HRs) of a B_7 texture nucleating from an isotropic phase; modified from Ref. [188]*; (c) Parental minimal surface of the HR in the shape of a ruled helicoid; (d) nested smectic layers built by translations from the parental helicoid. In part (c) and (d), the heliconical lines represent "columns" within the smectic layers; the layers and columns preserve parallelism and equidistance.*

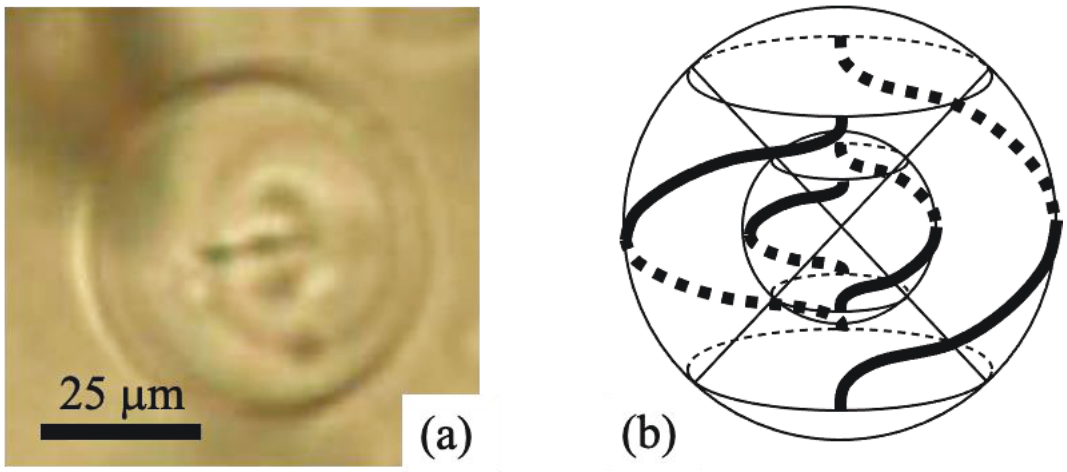

Figure 18: Kleman singular point developable domain: (a) apparent texture in a B_7 phase [188]; *(b) geometry of equidistant columns wrapped around concentric spherical surfaces.*

Small angle x-ray scattering (SAXS) [198,207,210,215] studies of materials showing the HR B_7 textures revealed a number of peaks [207,210] that can be indexed by a slightly oblique monoclinic 2D unit cell with *a*~3-5 nm and *b*~8-20 nm periodicities. These were interpreted as undulated layers [207,213,216] that form to avoid density modulation related to ferroelectric polarization splay and the tilted director structure. Later it was proposed that for some of these materials, the layers undulations are so strong that the layers break into small ribbons, which means that they can be considered as a columnar (originally known as B_1) phase. [210,217] Recent TEM observations of ~100 nm thick films showed that the layer undulations appearing in bulk as the consequence of the polarization splay can be suppressed in thin films. [218]

5. CONCLUSIONS

Small departures of molecules from the conventional rod shapes produce remarkable changes in self-assembly of LC phases, as demonstrated by the twist-bend nematic N_{TB}, helical nanofilament (HNF), dark conglomerate (DC), and the polarization modulated (B_7) phases. Topological defects in them show new features. For example, torical focal conic domains (TFCDs) that are ubiquitous in layered mesophases such as a thermotropic SmA, are of limited stability in the pseudolayered N_{TB}, transforming into parabolic focal conic domains (PFCDs) [16]. Furthermore, in SmA and lyotropic lamellar phases, generic FCDs of nonzero eccentricity emit edge dislocations that are clearly discernable under a polarizing optical microscope, while in N_{TB}, these dislocations are not

visible. Kleman and Krishnamurthy suggested that the plausible reasons might be an "infinitesimal imperfect" character of the dislocations or a small nanoscale value of their Burgers vectors [16]. Another important feature predicted for FCDs in N_{TB} is that they should emit disclinations [16], an effect known for FCDs in SmC, but not in SmA. One of the most notable scientific achievements of Maurice Kleman was the development of homotopy classification of defects in ordered media [45–47], which connects the type of ordering to the entire set of topologically permitted defects in it. For relatively simple phases, such as N_U, homotopy classification recovers results that have been already obtained by a more laborious analysis of the elastic energy. Examples are the escape of $k = 1$ disclinations into the third dimension and mutual equivalency of all half-integer disclinations. The true power of homotopy classification is revealed when the organization is more complex, which is the case of superfluid phases of He-3 [65] and biaxial nematic N_B [68]. The homotopy classification predicts that two 1/2 disclinations crossing each other in N_B might leave a third disclination of a strength 1 that connects the two initial ones [68]. Observation of this event would be an unambiguous proof of the biaxial order since in a uniaxial N_U, the disclinations cross each other freely.

In the examples above, topological defects appear as departures from the equilibrium uniformly aligned states, stabilized by surface anchoring, external fields, or trapped in metastable states while relaxing from an externally induced perturbation. In some cases, defects serve as a building unit of an equilibrium bulk structure, relieving frustrations between competing tendencies, such as a double twist and space tiling in blue phases. Bent-core materials show a rich spectrum of phases with defects. In particular, the DC phase could be considered as a mesh of interconnected and disoriented small TFCDs of negative Gaussian curvature of molecular layers [107]. HNF and B_7 phases show similar motifs of helicoidally nested smectic layers, albeit on different length scales, hundreds of nanometers and tens of micrometers, respectively. Their structures, deciphered only recently, bears a strong similarity to the model of screw dislocation of a giant Burgers vector, proposed by Maurice Kleman on the ground of geometrical and elastic properties of layered liquid crystals. Not surprisingly, the generality of geometrical constructions discovered in liquid crystals extends to other systems, most notably those of biological origin. In particular, the helical ribbon structures bear similarity to Kleman's model [30] of DNA packings in chromosomes of Dinoflagellate, in which the DNA molecules, aligned along the straight lines in Figure 17c,d, combine twist with 2D periodic translational order.

We expect that knowledge uncovered so far in the studies of defects in bent-core liquid crystals, to which Maurice Kleman contributed greatly, will be of inspirational help in the studies of other complex materials.

5. ACKNOWLEDGEMENTS:

AJ acknowledges financial support by the National Science Foundation (NSF) under grants DMR-1904167 and DMR-1904091. YuN achnowledges support by Hetman Petro Sahaidachnyi National Army Academy (Ukraine). ODL research is supported by NSF grants DMR-1905053, DMS-2106675, ECCS-190610, ECCS-2122399, and by the Office of Sciences, DOE, grant DESC0019105.

REFERENCES

[1] Friedel G. Les états mésomorphes de la matière. Ann phys. 1922;18:273–315.

[2] de Gennes PG, Prost J. The Physics of Liquid Crystals. 2nd ed. Oxford: Claredon Press; 1993.

[3] M. Kleman. Points, Lines and Walls: In Liquid Crystals, Magnetic Systems and Various Ordered Media. Chichester; 1983.

[4] Kleman M, Lavrentovich OD. Soft Matter Physics: An Introduction. Partially Ordered Systems. L. Lam, editor. New York: Springer; 2003.

[5] Friedel J, Kleman M. Application of dislocation theory to liquid crystals. In: Simmons JA, Bullough R, editors. Fundam Asp dislocation theory. Washington, D.C.: US National Bureau of Standards; 1970. p. 607–636.

[6] Kléman M. Defects and their relationship to molecular configurations in nematic polymers. Faraday Discuss Chem Soc. 1985;79:215–224.

[7] OD L, M K. Cholesteric Liquid Crystals: Defects and Topology, in 2001, Springer-Verlag: New York. p. In: HS. K, C B, editors. Chirality Liq Cryst. New York: Springer-Verlag; 2001. p. 115–158.

[8] Kleman M, Lavrentovich O, Nastishin Y. Dislocations and Disclinations in Mesomorphic Phases. In: Nabarro F, Hirst J, editors. Dislocations Solids ,V 12. Elsevier B.V; 2004. p.

150–265.

[9] Kleman M, Lavrentovich OD. Topological point defects in nematic liquid crystals. Philos Mag. 2006;86:4117–4137.

[10] Kleman M, Lavrentovich OD. Liquids with conics. Liq Cryst. 2009;36:1085–1099.

[11] Kleman M, Friedel J. Disclinations, dislocations, and continuous defects: A reappraisal. Rev Mod Phys. 2008;80:61–115.

[12] Achard MF, Kleman M, Nastishin YA, et al. Liquid crystal helical ribbons as isometric textures. Eur Phys J E. 2005;16:37–47.

[13] Kleman M, Friedel J. Lignes de dislocation dans les cholestériques. J Phys Colloq. 1969;30:C4-43-C4-53.

[14] Bouligand Y, Kléman M. , Helical Disclination Pairs in Cholesteric Mesophases. J Phys-Paris. 1970;31:1041–1054.

[15] Cladis PE, Kléman M. Non-singular disclinations of strength S = + 1 in nematics. J Phys. 1972;33:591–598.

[16] Kleman M, Krishnamurthy KS. Defects in the twist-bend nematic phase: Stabilities and instabilities of focal conic domains and related topics. Phys Rev E. 2018;98:032705.

[17] De'Neve T, Kleman M, Navard P. Defect morphology in a biaxial thermotropic polymer. J Phys II. 1992;2:187–207.

[18] Kléman M, Williams CE. Interaction between Parallel Edge Dislocation Lines in a Smectic a Liquid-Crystal. J Phys Lett-Paris. 1974;35:L49–L51.

[19] M. Kleman, Williams CE, Costello MJ, et al. Defect Structures in Lyotropic Smectic Phases Revealed by Freeze-Fracture Electron-Microscopy. Philos Mag. 1977;35:33–56.

[20] Kleman M. Elasticity and Defects in a Smectic-C Phase. Ann Phys-Paris. 1978;3:265–265.

[21] Bouligand Y, Kleman M. Topology of Singular Lines in Non-Chiral Smectics. J Phys-Paris. 1979;40:79–97.

[22] Allain M, Kleman M. Thermodynamic Defects, Instabilities and Mobility Processes in the

Lamellar Phase of a Nonionic Surfactant. J Phys-Paris. 1987;48:1799–1807.

[23] Bourdon L, Kleman M, Lejcek L, et al. On Static Helical Instabilities of Screw Dislocations in a Sma Phase and on Their Consequence on Plasticity. J Phys-Paris. 1981;42:261–268.

[24] Meyer C, Nastishin Y, Kleman M. Helical defects in smectic- A and smectic- A phases. Phys Rev E - Stat Nonlinear, Soft Matter Phys. 2010;82: 031704-1–12.

[25] Meyer C, Logbo H, Briouel B, et al. Double helical defects in smectic a and smectic A* phases. Liq Cryst. 2010;37:1047–1057.

[26] Boltenhagen P, Lavrentovich O, Kleman M. Oily streaks and focal conic domains in L alpha lyotropic liquid crystals. J Phys II. 1991;1:1233–1252.

[27] Blanc C, M K. Curvature walls and focal conic domains in a lyotropic lamellar phase. Eur Phys J B. 1999;10:53–60.

[28] Kleman CB and M, Blanc C, Kleman M. The confinement of smectics with a strong anchoring. Eur Phys J E. 2001;4:241–251.

[29] Kléman M, Oswald P. Columnar discotic mesophases : elasticity , dislocations , instabilities. J Phys. 1982;43:655–662.

[30] Kléman M. The coexistence of cholesteric and 2-dimensional orders. J Phys. 1985;46:1193–1203.

[31] Nastishin YA, Kléman M, Malthête J, et al. Identification of a TGBA liquid crystal phase via its defects. Eur Phys J E. 2001;5:353–357.

[32] Kleman M, Yu.A. Nastishin, Malthête J. Defects in a TGBA phase: A theoretical approach. Eur Phys J E. 2002;8:67–78.

[33] Kleman M. Energetics of the Focal Conics of Smectic Phases. J Phys. 1977;38:1511–1518.

[34] Bourdon L, Sommeria J, Kleman M. On the Existence of Singular Lines in the Focal Domains of the Sm C and Sm C* Phases. J Phys-Paris. 1982;43:77–96.

[35] Sethna JP, Kleman M. Spheric Domains in Smectic Liquid-Crystals. Phys Rev A. 1982;26:3037–3040.

[36] Boltenhagen P, Kléman M, Lavrentovich O. Focal Conic Domains of Positive Gaussian Curvature in a Swollen Lamellar L-Alpha Phase. Comptes Rendus L Acad Des Sci Ser II. 1992;315:931–935.

[37] Boltenhagen P, Lavrentovich OD, Kléman M. Focal conic domains with positive Gaussian curvature and saddle-splay rigidity of smectic Lα phases. Phys Rev A. 1992;46.

[38] Lavrentovich OD, Kléman M, Pergamenshchik VM. Nucleation of Focal Conic Domains in Smectic A Liquid-Crystals. J Phys II. 1994;4:377–404.

[39] Blanc C, Kleman M. Tiling the plane with noncongruent toric focal conic domains. Phys Rev E - Stat Physics, Plasmas, Fluids, Relat Interdiscip Top. 2000;62:6739–6748.

[40] Kléman M, Lavrentovich OD. Grain boundaries and the law of corresponding cones in smectics. Eur Phys J E. 2000;2:47–57.

[41] Kleman M, Lavrentovich O. Curvature energy of a focal conic domain with arbitrary eccentricity. Phys Rev E. 2000;61:1574–1578.

[42] Nastishin YA, Meyer C, Kleman M. Imperfect focal conic domains in A smectics: A textural analysis. Liq Cryst. 2008;35:609–624.

[43] Kleman M. Developable Domains in Hexagonal Liquid Crystals. J Phys Paris. 1980;41:737–745.

[44] Oswald P, Kléman M. Défauts dans une mésophase hexagonale discotique : disinclinaisons et parois. J Phys-Paris. 1981;42:1461–1472.

[45] Toulouse G, Kléman M. Principles of a Classification of Defects in Ordered Media. Basic Notions Condens Matter Phys. 2018;37:389–391.

[46] Kléman M, Michel L, Toulouse G. Classification of topologically stable defects in ordered media. J Phys Lettres. 1977;38:195–197.

[47] KLÉMAN M, MICHEL L. Spontaneous Breaking of Euclidean Invariance and Classification of Topologically Stable Defects and Configurations of Crystals and Liquid Crystals Maurice. Phys Rev Lett. 1978;40:1387–1390.

[48] Krishnamurthy KS, Tadapatri P, Weissflog W. Twist disclination loops in a bent-core

nematic liquid crystal. Soft Matter. 2011;7:6273–6284.

[49] Friedel J, Gennes PG de. Disclination Loops in Liquid Crystals. Cr Acad Sci B Phys. 1969;268:257.

[50] Pardaev SA, Williams JC, Twieg RJ, et al. Polar structure of disclination loops in nematic liquid crystals probed by second harmonic light scattering. Phys Rev E. 2015;91:032501.

[51] Helfrich W. Alignment-inversion walls in nematic liquid crystals in the presence of a magnetic field. Phys Rev Lett. 1968;21:1518–1521.

[52] Aharoni A. Introduction to the theory of ferromagnetism. Oxford, New York: Clarendon Press; Oxford University Press; 1996.

[53] Meyer RB. Piezoelectric effects in liquid crystals. Phys Rev Lett. 1969;22:918–921.

[54] Li B-X, Nastishin YA, Wang H, et al. Liquid crystal phases with unusual structures and physical properties formed by acute-angle bent core molecules. Phys Rev Res. 2020;2:33371.

[55] Jákli A, Lavrentovich OD, Selinger J V. Physics of liquid crystals of bent-shaped molecules. Rev Mod Phys. 2018;90:045004.

[56] Freiser MJ. Ordered States of a Nematic Liquid. Phys Rev Lett. 1970;24:1041–1043.

[57] Li J-F, Rosenblatt C, Lavrentovich OD, et al. Biaxiality in a Cyclic Thermotropic Nematic Liquid Crystal. Eur Lett. 1994;25:199–204.

[58] Niori T, Sekine T, Watanabe J, et al. Distinct ferroelectric smectic liquid crystals consisting of banana shaped achiral molecules. J Mater Chem. 1996;6:1231–1233.

[59] Van Le K, Mathews M, Chambers M, et al. Electro-optic technique to study biaxiality of liquid crystals with positive dielectric anisotropy: The case of a bent-core material. Phys Rev E. 2009;79:030701.

[60] Senyuk B, Wonderly H, Mathews M, et al. Surface alignment, anchoring transitions, optical properties, and topological defects in the nematic phase of thermotropic bent-core liquid crystal A131. Phys Rev E. 2010;82:041711–041713.

[61] Kim Y-K, Cukrov G, Xiang J, et al. Domain walls and anchoring transitions mimicking nematic biaxiality in the oxadiazole bent-core liquid crystal C7. Soft Matter. 2015;11:3963–3970.

[62] Kim Y-K, Senyuk B, Lavrentovich OD. Molecular reorientation of a nematic liquid crystal by thermal expansion. Nat Commun. 2012;3:1133.

[63] Kim Y-KY-K, Majumdar M, Senyuk BI, et al. Search for biaxiality in a shape-persistent bent-core nematic liquid crystal. Soft Matter. 2012;8:8880.

[64] Meyer RB. Existence of even indexed disclinations in nematic liquid crystals. Philos Mag. 1973;27:405–424.

[65] Volovik GE, Mineyev VP. Investigation of Singularities in Superfluid He-3 and Liquid-Crystals by Homotopic Topology Methods. Zhurnal Eksp I Teor Fiz. 1977;72:2256–2274.

[66] Volovik GE, Lavrentovich OD. Topological dynamics of defects: boojums in nematic drops. Sov Phys JETP. 1983;58:1159–1166.

[67] Harkai S, Cordoyannis G, Susser AL, et al. Manipulation of mechanically nanopatterned line defect assemblies in plane-parallel nematic liquid crystals. Liq Cryst Rev. 2022; in press.

[68] Toulouse G. Pour les n ´ematiques biaxes To cite this version : J Phys Lettres. 1977;38:67–68.

[69] Ishikawa T, Lavrentovich OD. Crossing of disclinations in nematic slabs. Europhys Lett. 1998;41:171–176.

[70] Dirac PAM. Quantised singularities in the electromagnetic field. P R Soc L a-Conta. 1931;133:60–72.

[71] Kurik M V., Lavrentovich OD. Defects in Liquid-Crystals - Homotopy-Theory and Experimental Investigations. Sov Phys Uspekhi. 1988;31:196–224.

[72] Senyuk B, Kim YK, Tortora L, et al. Surface alignment, anchoring transitions, optical properties and topological defects in nematic bent-core materials C7 and C12. Mol Cryst Liq Cryst. 2011;540:20–41.

[73] Cestari M, Diez-Berart S, Dunmur DA, et al. Phase behavior and properties of the liquid-crystal dimer 1″,7″-bis(4-cyanobiphenyl-4′-yl) heptane: A twist-bend nematic liquid crystal. Phys Rev E. 2011;84:031704.

[74] Chen D, Porada JH, Hooper JB, et al. Chiral heliconical ground state of nanoscale pitch in a nematic liquid crystal of achiral molecular dimers. Proc Natl Acad Sci. 2013;110:15931–15936.

[75] Borshch V, Kim Y-K, Xiang J, et al. Nematic twist-bend phase with nanoscale modulation of molecular orientation. Nat Commun. 2013;4:2635-1–8.

[76] Meyer RB. Macroscopic phenomena in nematic polymers. In: Ciferri A, Krigbaum WR, Meyer RB, editors. Polym Liq Cryst. New York/London: Academic Press, Inc.; 1982. p. 133–185.

[77] Dozov I. On the spontaneous symmetry breaking in the mesophases of achiral banana-shaped molecules. Eur Lett. 2001;56:247–253.

[78] Memmer R. Liquid crystal phases of achiral banana-shaped molecules: a computer simulation study. Liq Cryst. 2002;29:483–496.

[79] Meyer RB. Effects of electric and magnetic fields on the structure of cholesteric liquid crystals. Appl Phys Lett. 1968;12:281–282.

[80] De Gennes PG. Calcul de la distorsion d'une structure cholesterique par un champ magnetique. Solid State Commun. 1968;6:163–165.

[81] Xiang J, Shiyanovskii S V., Imrie C, et al. Electrooptic Response of Chiral Nematic Liquid Crystals with Oblique Helicoidal Director. Phys Rev Lett. 2014;112:217801.

[82] Salili SM, Xiang J, Wang H, et al. Magnetically Tunable Selective Reflection of Light by Heliconical Cholesterics. Phys Rev E. 2016;94:042705.

[83] Pieranski P. Cholesteric dislocations in mica wedges. Liq Cryst Rev. 2022; in press.

[84] Wu ST, Smalyukh II. Review: Hopfions, heliknotons, skyrmions, torons and both abelian and nonabelian vortices in chiral liquid crystals. Liq Cryst Rev. 2022; in press.

[85] Panov V, Nagaraj M, Vij J, et al. Spontaneous Periodic Deformations in Nonchiral Planar-

Aligned Bimesogens with a Nematic-Nematic Transition and a Negative Elastic Constant. Phys Rev Lett. 2010;105:167801.

[86] Dawood AA, Grossel MC, Luckhurst GR, et al. On the twist-bend nematic phase formed directly from the isotropic phase. Liq Cryst. 2016;43:2–12.

[87] Babakhanova G, Parsouzi Z, Paladugu S, et al. Elastic and viscous properties of the nematic dimer CB7CB. Phys Rev E. 2017;96:062704.

[88] Challa PK, Borshch V, Parri O, et al. Twist-bend nematic liquid crystals in high magnetic fields. Phys Rev E. 2014;89:060501 (R)-1–5.

[89] You R, Paterson DA, Storey JMD, et al. Formation of periodic zigzag patterns in the twist-bend nematic liquid crystal phase by surface treatment. Liq Cryst. 2017;44:168–176.

[90] Panov VP, Sreenilayam SP, Panarin YP, et al. Characterization of the sub-micrometer hierarchy levels in the twist-bend nematic phase with nanometric helices via photopolymerization. Explanation for the sign reversal in the polar response. Nano Lett. 2017;17:7515–7519.

[91] Simpson FFP, Mandle RJ, Moore JN, et al. Investigating the Cusp between the nano- and macro-sciences in supermolecular liquid-crystalline twist-bend nematogens. J Mater Chem C. 2017;5:5102–5110.

[92] Eremin A, Nádasi H, Kurochkina M, et al. Light-Responsive Microstructures in Droplets of the Twist-Bend Nematic Phase. Langmuir. 2018;34:14519–14527.

[93] Jakli A, Saupe A. Spontaneous transition from chevron to striped texture of a planar smectic C* liquid crystal. Phys Rev A. 1992;45:5674–5680.

[94] Subacius D, Voloschenko D, Bos P, et al. Preliminary communication Modulated structures with field-controlled direction and periodicity in SmC liquid crystals Preliminary com munication M odulated structures with ® eld-controlled direction and periodicity in Sm C * liquid crystals. Liq Cryst. 1999;26:295–298.

[95] Kleman M. Chronologies d'un physician. Paris: Calvage & Mounet; 2016.

[96] Friedel G, Grandjean F. Observations géométriques sur les liquides á conique focales. Bull

Soc Fr Minéral. 1910;33:409–465.

[97] J. Friedel. Dislocation. Oxford: Pergamon Press; 1964.

[98] Krishnamurthy KS, Kanakala MB, Yelamaggad C V., et al. Instabilities in the electric Freedericksz state of the twist-bend nematic liquid crystal CB7CB. Soft Matter. 2018;14:5393–5406.

[99] Krishnamurthy KS, Rao DSS, Kanakala MB, et al. Topological defects due to twist-bend nematic drops mimicking colloidal particles in a nematic medium. Soft Matter. 2020;16:7479–7491.

[100] Bragg W. Liquid Crystal. Nature. 1934;133:445–446.

[101] Bidaux R, Boccara N, Sarma G, et al. Statistical properties of focal conic textures in smectic liquid crystals. J Phys. 1973;34:661–672.

[102] Lavrentovich D. Hierarchy of defect structures in space filling by flexible smectic-A layers. Sov Phys JETP. 1986;984–990.

[103] Lavrentovich OD, Kleman M. Field-driven first-order structural transition in restricted geometry of a smectic-A cell. Phys Rev E. 1993;48:R39–R42.

[104] Rosenblatt CS, Pindak R, Clark NA, et al. The parabolic focal conic : a new smectic a defect. J Phys Fr. 1977;38:1105–1115.

[105] W.R. Folks T.A. Krentzel, B. Zalar, H. Zeng, Yu. A. Reznikov, M. Neubert, S. Kumar, D. Finotello and O.D. Lavrentovich SK. Photocontrol of Smectic Spacing. Mol Cryst Liq Cryst. 1998;320:77–88.

[106] Smalyukh II, Pratibha R, Madhusudana N V., et al. Selective imaging of 3D director fields and study of defects in biaxial smectic A liquid crystals. Eur Phys J E. 2005;16:179–191.

[107] Hough LE, Spannuth M, Nakata M, et al. Chiral isotropic liquids from achiral molecules. Science. 2009;325:452–456.

[108] Chen D, Shen Y, Zhu C, et al. Interface structure of the dark conglomerate liquid crystal phase. Soft Matter. 2011;7:1879.

[109] Chen D, Shao R, Maclennan JE, et al. Topography of bent-core liquid crystals at the air/liquid crystal interface. Liq Cryst. 2013;40:1730–1735.

[110] Chen D, Heberling M-S, Nakata M, et al. Structure of the B4 liquid crystal phase near a glass surface. ChemPhysChem. 2012;13:155–159.

[111] Paterson DA, Xiang J, Singh G, et al. Reversible Isothermal Twist−Bend Nematic−Nematic Phase Transition Driven by the Photoisomerization of an Azobenzene- Based Nonsymmetric Liquid Crystal Dimer. J Am Chem Soc. 2016;138:5283–5289.

[112] Feng C, Feng J, Saha R, et al. Manipulation of the nanoscale heliconical structure of a twist-bend nematic material with polarized light. Phys Rev Res Rapid Commun. 2020;2:032004(R).

[113] Dozov I, Meyer C. Analogy between the twist-bend nematic and the smectic A phases and coarse-grained description of the macroscopic N TB properties. Liq Cryst. 2017;44:4–23.

[114] Meyer C, Stoenescu D, Luckhurst GR, et al. Smectic-like bâtonnets in nematic/twist-bend nematic biphasic samples. Liq Cryst. 2017;44.

[115] Meyer C, Dozov I. Local distortion energy and coarse-grained elasticity of the twist-bend nematic phase. Soft Matter. 2016;12:574–580.

[116] Lavrentovich OD. Filling of Space by Flexible Smectic Layers. Mol Cryst Liq Cryst Inc Nonlinear Opt. 1987;151:417–424.

[117] Fournier JB, Durand G. Focal conic faceting in smectic-A liquid crystals. J Phys II. 1991;1:845–870.

[118] Fournier JB, Dozov I, Durand G. Surface frustration and texture instability in smectic-A liquid crystals. Phys Rev A. 1990;41:2252–2255.

[119] Meyer C, Cunff L Le, Belloul M, et al. Focal conic stacking in smectic a liquid crystals: Smectic flower and apollonius tiling. Materials (Basel). 2009;2:499–513.

[120] Honglawan A, Beller D a., Cavallaro M, et al. Pillar-assisted epitaxial assembly of toric focal conic domains of smectic-A liquid crystals. Adv Mater. 2011;23:5519–5523.

[121] Honglawan A, Beller DA, Cavallaro M, et al. Topographically induced hierarchical

assembly and geometrical transformation of focal conic domain arrays in smectic liquid crystals. Proc Natl Acad Sci U S A. 2013;110:34–39.

[122] Beller D a., Gharbi M a., Honglawan A, et al. Focal conic flower textures at curved interfaces. Phys Rev X. 2013;3:041026.

[123] Lavrentovich OD, Yang D. Cholesteric cellular patterns with electric-field-controlled line tension. Phys Rev E. 1998;57:R6269–R6272.

[124] Pardaev SA, Shamid SM, Tamba MG, et al. Second harmonic light scattering induced by defects in the twist-bend nematic phase of achiral liquid crystal dimers. Soft Matter. 2016;12:4472–4482.

[125] Scarbrough AN, Tuchband MR, Korblova ED, et al. The heliconical nematic twist-bend phase from “classic” bent-core benzylideneanilines with oligomethylene cores. Mol Cryst Liq Cryst. 2017;647:430–438.

[126] Perez A, Brunet M, Parodi O. Cofocal Conics in Smectics C. J Phys Lett. 1978;39:353–357.

[127] Perez A, Brunet M, Parodi O. Defects in Chiral Smectics-C .3. Surface Boundary Toric Defects. J Phys-Paris. 1981;42:1559–1568.

[128] Binysh J, Pollard J, Alexander GP. Geometry of Bend: Singular Lines and Defects in Twist-Bend Nematics. Phys Rev Lett. 2020;125:47801.

[129] Volovik GE, Lavrentovich OD. The Topological Dynamics of Defects - Boojums in Nematic Drops. Zh Eksp Teor Fiz. 1983;85:1997–2010.

[130] Kurik M V., Lavrentovich OD. Monopole structures and shape of drops of smectics-C. Sov Phys JETP. 1983;58:299–307.

[131] Lavrentovich OD. Topological defects in dispersed words and worlds around liquid crystals, or liquid crystal drops. Liq Cryst. 1998;24:117–126.

[132] Urbanski M, Reyes CG, Noh J, et al. Liquid crystals in micron-scale droplets, shells and fibers. J Phys Condens Matter. 2017;29.

[133] Lopez-Leon T, Fernandez-Nieves A. Drops and shells of liquid crystal. Colloid Polym Sci. 2011;289:345–359.

[134] Li Y, Jun-Yan Suen J, Prince E, et al. Colloidal cholesteric liquid crystal in spherical confinement. Nat Commun. 2016;7.

[135] Krishnamurthy KS, Shankar Rao DS, Kanakala MB, et al. Electric response of topological dipoles in nematic colloids with twist-bend nematic droplets as the dispersed phase. Phys Rev E. 2021;103:1–10.

[136] Oswald P, Dequidt A, Poy G. Lehmann effect in nematic and cholesteric liquid crystals: a review. Liq Cryst Rev. 2019;7:142–166.

[137] Lavrentovich O, Nastishin Y. Division of drops of a liquid crystal in the case of a cholesteric-smectic-A phase transition. Sov Phys JETP Lett. 1984;40:1015–1019.

[138] Muševič I. Liquid-crystal micro-photonics. Liq Cryst Rev. 2016;4:1–34.

[139] Hernández RJ, Provenzano C, Mazzulla A, et al. Cholesteric solid spherical microparticles: Chiral optomechanics and microphotonics. Liq Cryst Rev. 2016;4:59–79.

[140] Carlton RJ, Hunter JT, Miller DS, et al. Chemical and biological sensing using liquid crystals. Liq Cryst Rev. 2013;1:29–51.

[141] Robinson C. Liquid-Crystalline Structures in Solutions of Polypeptide. Trans Faraday Soc 52, 571-592. 1955;

[142] Robinson C, Ward JC, Beevers RB. Liquid crystalline structure in Polypeptide solutions. Part 2. Faraday Soc. 1958;25:29.

[143] Kurik M V., Lavrentovich OD. Negative-Positive Monopole Transitions in Cholesteric Liquid-Crystals. Sov Phys JETP Lett. 1982;35:444–447.

[144] Li Y, Prince E, Cho S, et al. Periodic assembly of nanoparticle arrays in disclinations of cholesteric liquid crystals. Proc Natl Acad Sci U S A. 2017;114:2137–2142.

[145] Seč D, Porenta T, Ravnik M, et al. Geometrical frustration of chiral ordering in cholesteric droplets. Soft Matter. 2012;8:11982–11988.

[146] Eremin A. Effects of photoswitching in complex partially ordered systems. Liq Cryst Rev. 2020;8:29–43.

[147] Lavrentovich OD. Design of nematic liquid crystals to control microscale dynamics. Liq Cryst Rev. 2020;8:59–129.

[148] Yoshioka J, Salamon P, Paterson DA, et al. Spherical-cap droplets of a photo-responsive bent liquid crystal dimer. Soft Matter. 2019;15:989–998.

[149] Liang HL, Schymura S, Rudquist P, et al. Nematic-smectic transition under confinement in liquid crystalline colloidal shells. Phys Rev Lett. 2011;106:1–4.

[150] Lopez-Leon T, Fernandez-Nieves A, Nobili M, et al. Nematic-smectic transition in spherical shells. Phys Rev Lett. 2011;106:2–5.

[151] Yun C-JJ, Vengatesan MR, Vij JK, et al. Hierarchical elasticity of bimesogenic liquid crystals with twist-bend nematic phase. Appl Phys Lett. 2015;106:173102.

[152] Reinitzer F. Beiträge zur Kenntniss des Cholesterins. Monatshefte für Chemie und verwandte Teile anderer Wissenschaften. 1888;9:421–441.

[153] Lehmann O. Scheinbar Lebende Fliessende Kristalle. Z Phys Chem. 1906;56:750.

[154] Gray GW. The Mesomorphic Behviour of the Fatty Acid Esters of Cholesterol. J Chem Soc. 1955;3733–3739.

[155] Saupe A. On Molecular Structure and Physical Properties of Thermotropic Liquid Crystals. Mol Cryst Liq Cryst. 1969;7:59–74.

[156] Brinkman SM and JPS and PWA and WF. Theory of the Blue Phase of Cholesteric Liquid Crystals. Phys Rev Lett. 1981;46:1216–1219.

[157] Meiboom S, Sammon M, Brinkman WF. Lattice of disclinations: The structure ofthe blue phases of cholesteric liquid crystals. Phys Rev A. 1983;27:438–454.

[158] Wright D, Mermin N. Crystalline liquids: the blue phases. Rev Mod Phys. 1989;61:385–432.

[159] Grelet E, Pansu B, Li M-H, et al. Structural Investigations on Smectic Blue Phases. Phys Rev Lett. 2001;86:3791–3794.

[160] Coles HJ, Pivnenko M. Liquid crystal “blue phases” with a wide temperature range. Nature.

2005;436:997–1000.

[161] Taushanoff S, Van Le K, Williams J, et al. Stable amorphous blue phase of bent-core nematic liquid crystals doped with a chiral material. J Mater Chem. 2010;20:5893.

[162] Renn SR, Lubensky TC. Abrikosov dislocation lattice in a model of the cholesteric-to-smectic- A transition. Phys Rev A. 1988;38:2132–2147.

[163] Gennes PG de. AN ANALOGY BETWEEN SUPERCONDLJCTORS AND SMECTICS A. Solid State Commun. 1972;10:753–756.

[164] Goodby JW, Waugh MA, Stein SM, et al. Characterization of a new helical smectic liquid crystal. Nature. 1989. p. 449–452..

[165] Longa L, Tomczyk W. Twist-bend nematic phase in the presence of molecular chirality. Liq Cryst. 2018;45:2074–2085.

[166] Longa L, Pająk G. Modulated nematic structures induced by chirality and steric polarization. Phys Rev E. 2016;93:040701(R) 1-5.

[167] Balachandran R, Panov VP, Panarin YP, et al. Flexoelectric behavior of bimesogenic liquid crystals in the nematic phase – observation of a new self-assembly pattern at the twist-bend nematic and the nematic interface. J Mater Chem C. 2014;2:8179–8184.

[168] Mandle RJ, Davis EJ, Archbold CT, et al. Microscopy studies of the nematic N TB phase of 1,11-di-(1″-cyanobiphenyl-4-yl)undecane. J Mater Chem C. 2014;2:556–566.

[169] Gorecka E, Vaupotič N, Zep A, et al. A Twist-Bend Nematic (N TB) Phase of Chiral Materials. Angew Chemie. 2015;54:10155–10159.

[170] Walker R, Pociecha D, Storey J, et al. The Chiral Twist-Bend Nematic Phase (N*TB). Chem - A Eur J. 2019;25:13329–13335.

[171] Salili SM, Ribeiro de Almeida RR, Challa PK, et al. Spontaneously modulated chiral nematic structures of flexible bent-core liquid crystal dimers. Liq Cryst. 2017;44:160–164.

[172] Walker R, Pociecha D, Salamończyk M, et al. Supramolecular liquid crystals exhibiting a chiral twist-bend nematic phase. Mater Adv. 2020;1:1622–1630.

[173] Mandle RJ, Goodby JW. A Novel Nematic-Like Mesophase Induced in Dimers, Trimers and Tetramers Doped with a Highly Chiral Additive. Soft Matter. 2018;14:8846–8852.

[174] Murachver MT, Nemati A, Salamończyk M, et al. Indication of a twist-grain-boundary-twist-bend phase of flexible core bent-shape chiral dimers. Soft Matter. 2019;15:3283–3290.

[175] Porte G, Gomati R, El Haitamy O, et al. Morphological transformations of the primary surfactant structures in brine-rich mixtures of ternary systems (surfactant/alcohol/brine). J Phys Chem. 1986;90:5746–5751.

[176] Nagaraj M. Dark conglomerate phases of bent-core liquid crystals. Liq Cryst. 2016;43:2244–2253.

[177] Ortega J, Folcia CL, Etxebarria J, et al. Interpretation of unusual textures in the B2 phase of a liquid crystal composed of bent-core molecules. Phys Rev E. 2003;68:011707.

[178] Pelzl G, Eremin A, Diele S, et al. Spontaneous chiral ordering in the nematic phase of an achiral banana-shaped compound. J Mater Chem. 2002;12:2591–2593.

[179] Jákli A, Huang Y-M, Fodor-Csorba K, et al. Reversible Switching Between Optically Isotropic and Birefringent States in a Bent-Core Liquid Crystal. Adv Mater. 2003;15:1606–1610.

[180] Liao G, Stojadinovic S, Pelzl G, et al. Optically isotropic ferroelectric liquid crystal phase. Phys.Rev. E*, 2005;*72**:** 021710

[181] Hough LE, Jung HT, Krueerke D, et al. Helical nanofilament phases. Science. 2009;325:456–460.

[182] Ryu SH, Kim H, Lee S, et al. Nucleation and growth of a helical nanofilament (B4) liquid-crystal phase confined in nanobowls. Soft Matter. 2015;11:7778–7782.

[183] Walba DM, Eshdat L, Körblova E, et al. On the Nature of the B4 Banana Phase : Crystal or Not a Crystal ? On the Nature of the B4 Banana Phase : Crystal or Not a. Cryst Growth Des. 2005;7483.

[184] Matsumoto EA, Alexander GP, Kamien RD. Helical Nanofilaments and the High Chirality

Limit of Smectics A. Phys Rev Lett. 2009;103:257804.

[185] Chen D, Heberling M-S, Nakata M, et al. Structure of the B4 liquid crystal phase near a glass surface. Chemphyschem. 2012;13:155–159.

[186] Sekine T, Niori T, Sone M, et al. Origin of helix in achiral banana-shaped molecular systems. Jpn J Appl Phys. 1997;36:6455–6463.

[187] Takanishi Y, Shin GJ, Jung JC, et al. Observation of very large chiral domains in a liquid crystal phase formed by mixtures of achiral bent-core and rod molecules. J Mater Chem. 2005;15:4020–4024.

[188] Nastishin YA, Nguyen HT, Kleman M, et al. Textural Analysis of a Mesophase with Banana Shaped Molecules. Eur Phys J E. 2003;12:581–591.

[189] Williams CE. Helical disclination lines in smectics a. Philos Mag. 1975;32:313–321.

[190] Zhang C, Diorio N, Lavrentovich OD, et al. Helical nanofilaments of bent-core liquid crystals with a second twist. Nat Commun. 2014;5:3302.

[191] Nakata M, Link DR, Araoka F, et al. A racemic layer structure in a chiral bent-core ferroelectric liquid crystal. Liq Cryst. 2001;28:1301–1308.

[192] Lin SC, Ho RM, Chang CY, et al. Hierarchical superstructures with control of helicity from the self-assembly of chiral bent-core molecules. Chem - A Eur J. 2012;18:9091–9098.

[193] Chen D, Tuchband MR, Horanyi B, et al. Diastereomeric liquid crystal domains at the mesoscale. Nat Commun. 2015;6:7763.

[194] Tsai E, Richardson JM, Korblova E, et al. A modulated helical nanofilament phase. Angew Chem Int Ed Engl. 2013;52:5254–5257.

[195] Li L, Salamonczyk M, Jákli A, et al. A Dual Modulated Homochiral Helical Nanofi lament Phase with Local Columnar Ordering Formed by Bent Core Liquid Crystals : Effects of Molecular Chirality. Small. 2016;12:3944–3955.

[196] Shadpour S, Nemati A, Salamończyk M, et al. Missing Link between Helical Nano- and Microfilaments in B4 Phase Bent-Core Liquid Crystals, and Deciphering which Chiral Center Controls the Filament Handedness. Small. 2020;16:1–12.

[197] Shadpour S, Nemati A, Boyd NJ, et al. Heliconical-layered nanocylinders (HLNCs) – hierarchical self-assembly in a unique B4 phase liquid crystal morphology. Mater Horizons. 2019;6:959–968.

[198] Pelzl G, Diele S, Jákli A, et al. Preliminary communication Helical superstructures in a novel smectic mesophase formed by achiral banana-shaped molecules. Liq Cryst. 1999;26:135–139.

[199] Pelzl G, Diele S, Jákli A, et al. The mysterious B7 phase: from its discovery up to the present stage of research. Liq Cryst. 2006;33:1513–1523.

[200] Jákli A, Krüerke D, Nair GG. Liquid crystal fibers of bent-core molecules. Phys Rev E. 2003;67:05170201–05170206.

[201] Nemeş A, Eremin A, Stannarius R, et al. Structure characterization of free-standing filaments drawn in the liquid crystal state. Phys Chem Chem Phys. 2006;8:469–476.

[202] Eremin A, Nemeş A, Stannarius R, et al. Structure and mechanical properties of liquid crystalline filaments. Phys Rev E. 2005;71:31705.

[203] Stannarius R, Nemeş A, Eremin A. Plucking a liquid chord: Mechanical response of a liquid crystal filament. Phys Rev E 2005;72:020702.

[204] Eremin A, Kornek U, Stern S, et al. Pattern-Stabilized Decorated Polar Liquid-Crystal Fibers. Phys Rev Lett. 2012;109:017801–017805.

[205] Bailey CA, Jákli A. Role of Molecular Shape on Bent-Core Liquid-Crystal Structures. Phys Rev Lett. 2007;99:207801.

[206] Jákli A, Krüerke D, Sawade H, et al. Evidence for Triclinic Symmetry in Smectic Liquid Crystals of Bent-Shape Molecules. Phys Rev Lett. 2001;86:5715–5718.

[207] Coleman DA, Fernsler J, Chattham N, et al. Polarization-Modulated Smectic Liquid Crystal Phases. Science. 2003;301:1204–1211.

[208] Pelzl G, Schroder MW, Dunemann U, et al. The first bent-core mesogens exhibiting a dimorphism B 7-SmCP A. J Mater Chem. 2004;14:2492–2498.

[209] Vaupotič N, Čopič M, Gorecka E, et al. Modulated Structures in Bent-Core Liquid Crystals:

Two Faces of One Phase. Phys Rev Lett. 2007;98:247802.

[210] Folcia C, Etxebarria J, Ortega J, et al. Structure of mesogens possessing B7 textures: The case of the bent-core mesogen 8-OPIMB-NO_{2}. Phys Rev E 2005;72:041709.

[211] Vaupotič N, Čopič M. Polarization modulation instability in liquid crystals with spontaneous chiral symmetry breaking. Phys Rev E. 2005;72:031701.

[212] Coleman DA, Jones CD, Nakata M, et al. Polarization splay as the origin of modulation in the B1 and B7 smectic phases of bent-core molecules. Phys Rev E. 2008;77:21703.

[213] Vaupotič N, Čopič M, Gorecka E, et al. Modulated Structures in Bent-Core Liquid Crystals: Two Faces of One Phase. Phys Rev Lett. 2007;98:247802.

[214] D.H. van Winkle, Clark NA. Freely Suspended Strands of Tilted Columnar Liquid-Crystal Phases: One-Dimensional Nematics with Orientational Jumps. Phys Rev Lett. 1982;48:1407–1410.

[215] Zhang C, Diorio N, Radhika S, et al. Two distinct modulated layer structures of an asymmetric bent-shape smectic liquid crystal. Liq Cryst. 2012;39:1149–1157.

[216] Vaupotič N, Čopič M. Polarization modulation instability in liquid crystals with spontaneous chiral symmetry breaking. Phys Rev E. 2005;72:031701.

[217] Pelzl G, Diele S, Weissflog W. Banana-Shaped Compounds -- A New Field of Liquid Crystals**. Adv Mater. 1999;11:707–724.

[218] Zhang C, Gao M, Almeida RRR De, et al. Polarization-Modulated Bent-Core Liquid Crystal Thin Films without Layer Undulation. Phys Rev Lett. 2019;122:137801.